



5-2014

## Kinetics of Formation and Oxidation of 8-oxo-7,8-dihydroguanine (8oxoG)

Derrick Ampadu Boateng  
*East Tennessee State University*

Follow this and additional works at: <https://dc.etsu.edu/etd>

 Part of the [Chemistry Commons](#)

---

### Recommended Citation

Ampadu Boateng, Derrick, "Kinetics of Formation and Oxidation of 8-oxo-7,8-dihydroguanine (8oxoG)" (2014). *Electronic Theses and Dissertations*. Paper 2314. <https://dc.etsu.edu/etd/2314>

This Thesis - unrestricted is brought to you for free and open access by the Student Works at Digital Commons @ East Tennessee State University. It has been accepted for inclusion in Electronic Theses and Dissertations by an authorized administrator of Digital Commons @ East Tennessee State University. For more information, please contact [digilib@etsu.edu](mailto:digilib@etsu.edu).

Kinetics of Formation and Oxidation of 8-oxo-7,8-Dihydroguanine (8oxoG)

---

A thesis  
presented to  
the Faculty of the Department of Chemistry  
East Tennessee State University

In partial fulfillment  
of the requirements for the degree  
Master of Science in Chemistry

---

by  
Derrick Ampadu Boateng  
May 2014

---

Dr. Marina Roginskaya, Chair

Dr. Scott Kirkby

Dr. David Close

Keywords: 8-oxo-7,8-dihydroguanine; DNA damage; oxidative stress; reactive oxygen species;  
ionizing radiation; kinetics

## ABSTRACT

Kinetics of Formation and Oxidation of 8-oxo-7,8-Dihydroguanine (8oxoG)

by

Derrick Ampadu Boateng

8-oxo-7,8-dihydroguanine (8oxoG) is one of the most important base lesions formed during oxidative damage of DNA. The aim of the present research was to investigate the effects of DNA concentration, G content, and the nature of oxidizing species on the kinetics of 8oxoG in model DNA solutions by using HPLC. The experimentally obtained yields of 8oxoG were typically in the range of 2-2.5% of total concentration of guanine. The ratios of the rate constant of hole diffusion in DNA to the rate constant of conversion of the hole into 8oxoG ( $k_d/k_r$ ) were calculated from the experimental data using the diffusion model of charge transfer in DNA to be in the range of 200-300, in agreement with previously reported  $k_d/k_r$  ratios in the duplex DNA oligonucleotides  $(GGA)_n$  or  $(GGTT)_n$ . Our current diffusion model cannot satisfactorily explain the absence of the G content dependence of the 8oxoG yields, which indicates that a more advanced model is required.

## DEDICATION

My wife Josephine, my mother Akua Owusua, daughter Shanice, and my entire family.

## ACKNOWLEDGEMENTS

I am grateful to the almighty God for His guidance and protection throughout my life and especially during my graduate studies at ETSU. I thank my advisor Dr. Marina Roginskaya for her professional guidance and mentorship. My sincere gratitude goes to Dr. Scott Kirkby and Dr. David Close for serving on my committee and for their advice. I say thank you to Dr. Yuriy Razskazovski for his guidance. I thank Dr. Kamar Kutunpalli and Mrs. Mina McVeigh for their directions. I thank the staff of the Chemistry Department of ETSU, especially Dr. Mohseni, Mr. Ryan Alexander, Ms. Jillian Quirante, and Mr. Walt Witt.

My sincere gratitude goes to my sweet Mom who instilled in me the value of education, for her care and guidance which has brought me this far. My hearty appreciation goes to my wife and daughter Josephine and Shanice for their assured love and prayer during my studies and standing behind me through every situation. I thank my brother Prince and the wife Beianca for their tremendous support for me and my family.

I thank all graduate students in the Chemistry Department especially Josh Moore, my lab mate, for sharing ideas with me.

## TABLE OF CONTENTS

	Page
ABSTRACT .....	2
DEDICATION .....	3
ACKNOWLEDGEMENTS .....	4
LIST OF TABLES .....	9
LIST OF FIGURES .....	10
Chapter	
1. INTRODUCTION .....	14
Oxidative Stress and DNA .....	14
Charge Transfer.....	20
Superexchange.....	21
Hopping Mechanism.....	23
Previous Model of Long Distance Charge Transfer in DNA.....	24
The Diffusion Model of Competitive Electron Scavenging .....	24
General Principles of the Diffusion Model from Donor to Acceptor.....	28
Specific Aims.....	30
2. RATIONALE AND APPROACH.....	33
8oxoG Production by Various Oxidants.....	33
Hydroxyl Radical ( $\bullet\text{OH}$ ).....	35
Dibromide Radical Anion ( $\text{Br}_2\bullet^-$ ).....	36
Sulfate Radical Anion ( $\text{SO}_4\bullet^-$ ).....	37
Carbonate Radical Anion ( $\text{CO}_3\bullet^-$ ).....	37

Other Oxidants.....	38
Selenite Radical Anion $\text{SeO}_3^{\bullet-}$ .....	38
Thiocyanate Radical Anion $(\text{SCN})_2^{\bullet-}$ .....	39
The Effect of DNA Structure and G Content on 8oxoG Production.....	39
Analysis of Experimental Data on 8oxoG Kinetics Using the Diffusion Model of Hole Transfer in DNA.....	41
General Principles of the Diffusion Model of 8oxoG Kinetics.....	41
Mathematical Approach Using the Diffusion Model of Hole Transfer.....	44
3. <b>EXPERIMENTAL METHODS</b> .....	48
Instrumentation, Glassware, and Other Materials.....	48
Instrumentation.....	48
Glassware and Other Materials.....	48
Reagents Grade Stock Chemicals.....	49
Deoxyribonucleic Acids and Nucleobases.....	49
HPLC Solvents.....	49
Buffers, Solutions, and Gases.....	49
Other Reagents Used.....	50
Experimental Procedures.....	50
Samples Preparation.....	50
Preparation of DNA Solutions.....	50
Preparation of Stock Solutions.....	51
Determination of Extinction Coefficient of 8oxoG at 305 nm .....	52
Fricke Dosimetry.....	52

X-Irradiation Procedure and Illumination Procedures.....	53
DNA Hydrolysis.....	54
DNA Concentration Dependence Experiment.....	54
The Effect of Different DNA Hole Injectors.....	54
Oxygen Dependence Experiment.....	56
The Effect of Different DNA Content.....	56
HPLC Analysis.....	56
HPLC Analysis of Authentic 8oxoG as a Reference.....	56
HPLC Conditions for the Analysis of 8oxoG.....	57
Calculations of Concentrations of 8oxoG.....	57
4. RESULTS AND DISCUSSION.....	60
Optimizing Conditions for Quantitative Detection of 8oxoG.....	60
The rationale for using 305 nm as the wavelength for HPLC detection of guanine and 8oxoG.....	60
Determining the extinction coefficient of 8oxoG at 305nm.....	61
Linearity of 8oxoG.....	62
Fricke Dosimetry.....	63
Optimizing of HPLC Conditions for Detection of 8oxoG.....	64
The Effect of DNA Concentration on Production of 8oxoG.....	68
The Effect of the Nature of Different Oxidant on the Production of 8oxoG.....	73
Dibromide Radical Anion, Br <sub>2</sub> <sup>•-</sup> .....	73



	Hydroxyl Radical $\bullet\text{OH}$ .....	74
	Sulfate Radical Anion $\text{SO}_4^{\bullet-}$ .....	76
	Carbonate Radical Anion, $\text{CO}_3^{\bullet-}$ .....	78
	Other Oxidants: $\text{SeO}_3^{\bullet-}$ and $(\text{SCN})_2^{\bullet-}$ .....	81
	The Effect of Oxygen on the Production of 8oxoG.....	82
	$\bullet\text{OH}$ Radical with and Without Oxygen.....	82
	$\text{Br}_2^{\bullet-}$ Radical with and Without Oxygen.....	83
	The Effect of G Content and Sequence of DNA on Production of 8oxoG.....	85
	The Effect of G Content on Production of 8oxoG.....	85
	The Effect of DNA Sequence on Production of 8oxoG.....	89
5.	CONCLUSION.....	91
	REFERENCES.....	93
	APPENDICES.....	101
	APPENDIX A: Determination of Extinction Coefficient of 8oxoG at 305nm..	101
	APPENDIX B: Fricke Dosimetry.....	102
	APPENDIX C: The Linear Regression for the Initial Accumulation of Different DNA Concentrations.....	103
	VITA .....	104

## LIST OF TABLES

Table	Page
1. Standard reduction potential of inorganic radicals .....	34
2. Standard reduction potentials of DNA bases in nucleosides.....	34
3. The experimentally determined extinction coefficients of DNA bases at 254 nm and 8oxoG and G at 305 nm in 40 mM ammonium acetate solution, pH 6.9.....	58
4. The radiation chemical yield of different DNA concentrations.....	69
5. Number of base pair per 8oxoG of different DNA.....	88
6. The ratios of the rate constant of diffusion to the rate constant of reaction for holes in DNA calculated from experimental data.....	90

## LIST OF FIGURES

Figure	Page
1. Reactions and products of guanine oxidation. The figure was created based on the reaction scheme shown in Close et al. ....	16
2. 8oxoG pairing with both adenine in the Hoogsteen base pairing and cytosine in the Classic Watson-Crick base pair.....	18
3. Chemical structures of various oxidized products of 8oxoG .....	19
4. Models of charge transfer in DNA: <b>A.</b> Superexchange, or tunneling mechanism for short distance charge transfer. <b>B.</b> Hopping mechanism for long-distance charge transfer.....	24
5. Diffusion model of migration of randomly injected electrons in brominated DNA.....	26
6. Schematic representation of Py sites as shallow electrons traps and T(OH)Br sites as deep electron traps.....	27
7. The diffusion model of charge migration from the donor to acceptor .....	29
8. Schematic representation of G sites as shallow hole traps and acceptor site as deep hole traps.....	29
9. An interstrand hopping between guanines located on the same strand separated by cytosine and zig-zag intrastrand hopping between guanines located on opposite strand in poly(GC-CG).....	40
10. An interstrand hopping between guanine located on the same strand in poly (GG- CC).....	40
11. The diffusion model of the hole transfer describing the formation and oxidation of	

8oxG in the DNA. $\delta$ is the distance between G; L is the average distance between neighboring 8oxoG; $L=N_{\text{bases}}/\delta$ .....	42
12. Schematic representation of G sites as shallow hole traps and 8oxoG at the terminals as deep electron traps.....	42
13. Graphical solution of Equation 12, where $y = 1-2\tanh(x)/x$ ; $x = \alpha/ X_{\infty}$ .....	46
14. The superimposition of the UV-Vis spectra of guanine (red trace) and 8oxoG (black).....	61
15. The linear regression of the absorbance of authentic 8oxoG solution in 40 mM ammonium acetate, pH 6.9 at 305 nm vs. absorbance at 285 nm.....	62
16. The calibration curve of the HPLC peak integrals of reference 8oxoG vs concentration of 8oxoG expressed as fold dilutions of saturated solution of 8oxoG.....	63
17. Fricke dosimetry dose-response curve. See the text and Appendix 2 for details.....	64
18. A representative chromatogram of a mixture of authentic 8oxoG and G. HPLC condition used: Reverse phase HPLC C18 column; equilibrated with 40mM ammonium acetate; linear gradient of acetonitrile from 0 to 8.8 % during 10 min at a flow rate of 1mL/min.....	65
19. Representative chromatogram shown at two different wavelengths (and on different scales) for 2 mM salmon testes DNA X-irradiated at 5.3 kGy 1 M NaBr in 10 mM phosphate, buffer pH 6.9 and then hydrolyzed in hot formic acid as described in Chapter 3. HPLC conditions are the same as in Figure 18.....	65
20. Accumulation of 8oxoG in an aqueous solution of salmon testes DNA irradiated in the presence of 1 M NaBr at various radiation times. Conditions: 2 mM (in bases) solution of DNA in 10 mM phosphate buffer, pH 6.9 was X- irradiated at indicated	

doses and then hydrolyzed in hot formic acid as described in Chapter 3.....	67
21. Yields of 8xoG as a function of dose for the following concentrations of salmon testes DNA (in nucleotides): <b>A.</b> 1mM; <b>B.</b> 2mM; <b>C.</b> 5mM; <b>D.</b> 10mM. DNA solutions were irradiated in the presence of 100 mM NaBr and then treated as described in Chapter 3.....	71
22. Accumulation of 8oxoG in X-irradiated salmon testes DNA for various concentrations of DNA. DNA was irradiated in the presence of 1 M NaBr and then treated as described in Chapter 3.....	72
23. Comparison of accumulation of 8oxoG produced as a result of DNA oxidation by hydroxyl radicals ( $\bullet\text{OH}$ ) and the dibromide radical anions ( $\text{Br}_2^{\bullet-}$ ). <b>A.</b> A total plot for $\bullet\text{OH}$ ; <b>B.</b> Total plots for $\text{Br}_2^{\bullet-}$ and $\bullet\text{OH}$ ; <b>C.</b> Initial regions for $\text{Br}_2^{\bullet-}$ and $\bullet\text{OH}$ .....	76
24. Accumulation of 8oxoG during DNA oxidation by $\text{SO}_4^{\bullet-}$ produced by photolysis using the Hg(Xe) lamp of aqueous solution persulfate during indicated times. HPLC conditions were as previously indicated.....	77
25. Accumulation of 8oxoG produced by DNA oxidation by $\text{CO}_3^{\bullet-}$ generated by: <b>A.</b> Photolysis of 2mM cobalt (III) pentaamminecarbonato perchlorate; <b>B.</b> Radiolysis of aqueous solution of 300 mM $\text{NaHCO}_3$ and 100 mM $\text{Na}_2\text{S}_2\text{O}_8$ .....	80
26. The effect of oxygen on the production of 8oxoG by hydroxyl radicals. Accumulation of 8oxoG from X-irradiated 10 mM solutions salmon testes DNA in the presence and absence of oxygen.....	83
27. The effect of oxygen on the production of 8oxoG by hydroxyl radicals. Accumulation of 8oxoG from X-irradiated 10 mM solutions of salmon testes DNA with 100 mM NaBr in the presence and absence of oxygen.....	84

28. Accumulation of 8oxoG from X-irradiated 2 mM solution of micrococcal DNA in 10 mM phosphate buffer, pH 6.9, in the presence of 1 M NaBr. Post irradiation treatment and HPLC conditions were as previously described.....	86
29. Accumulation of 8oxoG from X-irradiated 1 mM solution of poly (CG-GC). Other conditions are as in Figure 28.....	86
30. Accumulation of 8oxoG from X-irradiated 0.71 mM solution of poly(GG-CC). Other conditions are is in Figure 28. ....	87
31. The linear regression for the initial accumulation of different DNA concentrations, <b>A.</b> 1mM, <b>B.</b> 2mM, <b>C.</b> 5mM and <b>D.</b> 10mM .....	103

## CHAPTER 1

### INTRODUCTION

#### Oxidative Stress and DNA

Living organisms are constantly exposed to various exogenous insults such as environmental pollutants,<sup>1</sup> UV light,<sup>2</sup> ionizing radiation,<sup>3-5</sup> and tobacco smoke.<sup>6,7</sup> Collectively, all these agents contribute to overproduction of oxidizing species in the cells, the condition known as oxidative stress.<sup>8,9</sup> The species important for oxidative stress are known as *reactive oxygen species (ROS)*, such as  $\bullet\text{OH}$  (hydroxyl radical),  $\text{O}_2\bullet^-$  (superoxide radical),  $\text{H}_2\text{O}_2$  (hydrogen peroxide) and  $\text{CO}_3\bullet^-$  (carbonate radical). DNA, a major hereditary unit of living organisms, has been recognized as an important target for oxidative stress. Reactive species such as hydroxyl radicals,  $\bullet\text{OH}$ , are chief oxidants capable of oxidizing and causing damage to the DNA.<sup>10</sup> Oxidative damage to DNA can result in permanent mutation that promotes the development of cancer.<sup>10,11</sup> Oxidative damage to DNA also contributes to a broad spectrum of diseases such as inflammatory disease,<sup>12</sup> Alzheimer's disease,<sup>13,14</sup> Parkinson disease,<sup>15,16</sup> and ischemia and reperfusion.<sup>17</sup> It is also known to worsen conditions of existing illness such as leukemia<sup>18,19</sup> and also increase signs of aging.<sup>20</sup> DNA bases are the primary target of oxidation because of their lower oxidation potentials as compared to the DNA sugar-phosphate backbone.<sup>21</sup> Among the four bases in the DNA, (cytosine (C), thymine (T), guanine (G), and adenine (A), G is the most oxidizable because it has the lowest reduction potential (+1.29V).<sup>22-24</sup> One-electron oxidation of guanine in DNA produces *guanine radical cation* ( $\text{Gua}\bullet^+$  or  $\text{G}\bullet^+$ ), commonly known as DNA holes (Figure 1).<sup>25</sup> Compounds with a lower reduction potential such

as tryptophan are capable of reducing  $G^{\bullet+}$  (repairing of DNA damage)<sup>23</sup> with a rate constant of  $10^7 \text{ M}^{-1}\text{s}^{-1}$ . Other compounds such as 4-cyanophenol  $E^\circ = +1.17\text{V}$  with a rate constant of  $7.3 \times 10^5 \text{ M}^{-1}\text{s}^{-1}$ <sup>21</sup> and 4-aminophenol  $E^\circ = +0.14 \text{ V}$  with a rate constant of  $4.7 \times 10^9 \text{ M}^{-1}\text{s}^{-1}$ <sup>26</sup> are known to react with  $G^{\bullet+}$ . *Hoechst 3358*, a drug that reacts with  $G^{\bullet+}$  with a rate constant  $1.7 \times 10^9 \text{ M}^{-1}\text{s}^{-1}$  is also known to reduce  $G^{\bullet+}$ .<sup>21</sup>

$G^{\bullet+}$  is a significantly stronger acid ( $\text{pK}_a = 3.9$ , experimental values,<sup>27</sup> or  $3.6$  calculated<sup>28</sup>) than its parent  $G$  ( $\text{pK}_a = 9.5$ <sup>28</sup>), so it undergoes deprotonation to form  $G(\text{N1-H})^\bullet$ , also known as  $G^\bullet$ . However, this radical was not observed at room temperature and thus  $G^\bullet$  is believed to undergo the second one-electron oxidation to form a carbocation  $G(\text{N1-H})^+$ .<sup>28</sup> Hydrolysis of this carbocation produces 8-oxo-7,8-dihydroguanine (8oxoG). An alternative pathway of production of 8oxoG is via hydrolyses of  $G^{\bullet+}$  to form the  $G(\text{OH})^\bullet$  radical (Figure 1) that, in turn, can undergo further one-electron oxidation to form 8oxoG<sup>29,30</sup> or a one-electron reduction to form 2,6-diamino-4-hydroxy-5-formamidopyrimidine (FapyG).<sup>8,31-33</sup>



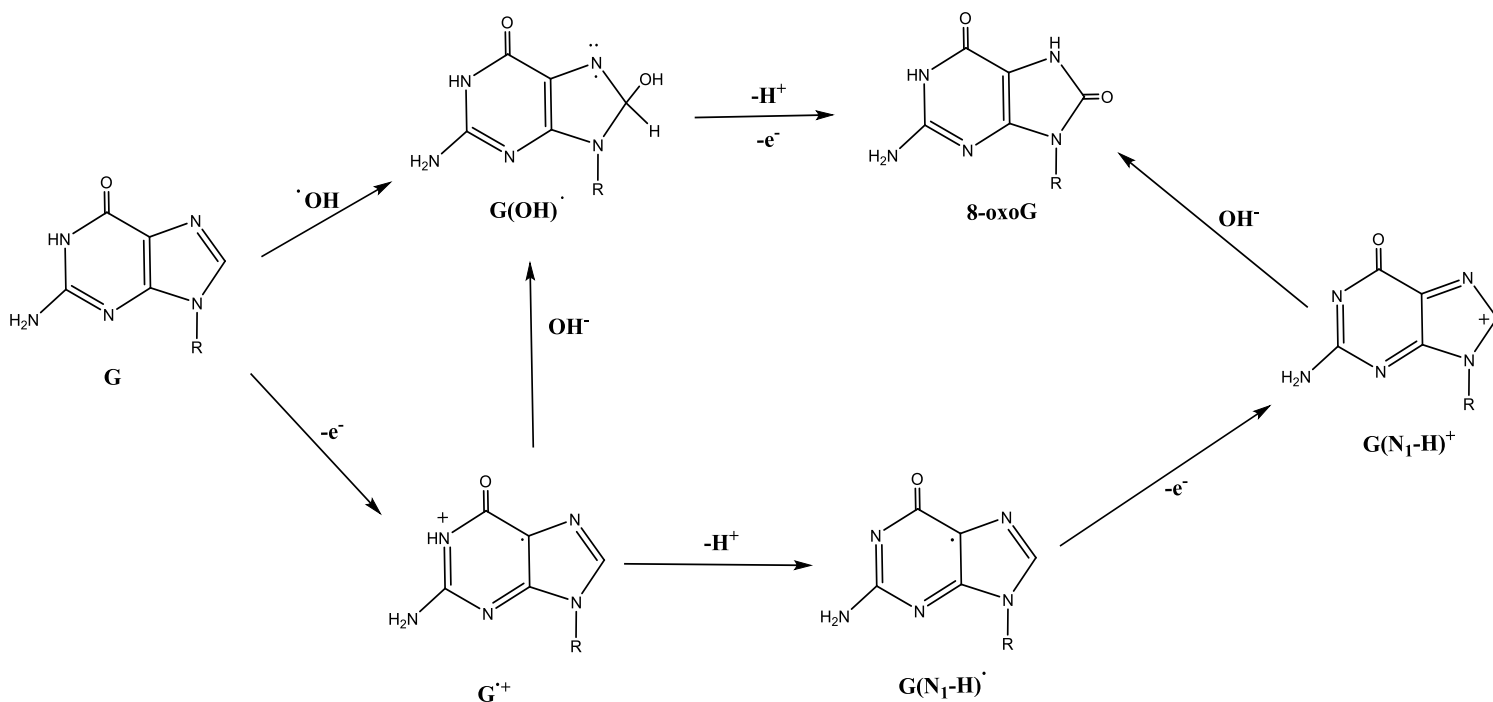


**Figure 1.** Reactions and products of guanine oxidation. The figure was created based on the reaction scheme shown in Close et al.<sup>35</sup>

It has been shown experimentally and theoretically that stretches of guanine ( $\text{G}_n$  sequences) in the DNA are even more easily oxidized.<sup>36</sup> This is due to the lower oxidation potential of the  $\text{G}_n$ <sup>22</sup> as compared to that of a single guanine (+1.29 V).<sup>22</sup> The GGG and GG are able to trap a hole with the probability equivalent to their oxidation potential.<sup>30,37-40</sup>  $\text{G}_n$  acts as a hole sink by scavenging migrating holes across the DNA  $\pi$  stack. Holes in DNA migrate until they reach a site with a lower oxidation potential (a deeper hole trap), such as GGG or GG where they react irreversibly via reactions shown in Figure 1. Thus these sequences are potentially mutagenic. Saito et al.<sup>36</sup> studied G-rich hot spots using photoinduced one-electron oxidation using different GG and GGG sequences in DNA oligonucleotides. The vulnerability of the  $\text{G}_n$  sequences was established in the order GGG > CGG > AGG: GGA > TGG > GGT > GGC:CGA

> AGA > TGA > CGT > AGT > CGC:TGT > AGC > TGC. The authors proposed that the sequence involving pyrimidine-G-pyrimidine is almost inert to photooxidation.

8oxoG is even a more efficient hole trap than guanine or (G)<sub>n</sub> because of its low oxidation potential 0.74V<sup>22</sup>, which is even lower than the oxidation potential of stretches of guanine (G<sub>n</sub>) that makes 8oxoG an oxidation hot spot.<sup>34</sup> It was first proposed by Doddridge et al.<sup>34</sup> that 8oxoG as a hot oxidation spot in DNA. They proved this by using a 8oxoG-containing DNA oligonucleotide with the sequence 5'-<sup>32</sup>P-ATGCATGCATXCATGCATGC-3', where X designates 8oxoG that was treated with aqueous piperidine after  $\gamma$ -irradiation. This group noticed one major band that was detected by polyacrylamide gel electrophoresis (PAGE). It turned out to be 8oxoG that was selectively cleaved in a dose-dependent fashion. This served as a clear indication of selective damage at the 8oxoG site in the DNA strand leading to a strand break even in the presence of other guanines. The group concluded on this finding that 8oxoG has the capacity of trapping holes even deeper and in a more efficient way as compared to the guanine stretch owing to its low reduction potential of 8oxoG.<sup>34</sup>

Over the years, research on the formation and further reactions of 8oxoG as biomarker of oxidative stress has been conducted.<sup>8,9,34</sup> Elevated levels of 8oxoG has been found in lungs<sup>41,42</sup> of people working or living in environments with high levels of asbestos fibers,<sup>43,44</sup> diesel exhaust particles,<sup>45</sup> and urban polluted areas that all caused an increase in lung cancer morbidity and cardiopulmonary mortality.<sup>46</sup> Heavy metals and some metalloids,<sup>47</sup> polycyclic aromatic hydrocarbons (PAH),<sup>48-51</sup> and others such as benzene, styrene, and organic arsenic were all associated with elevated levels of 8oxoG due to the oxidative stress.<sup>45</sup>

8oxoG is a mutagenic lesion that can form not only the classic Watson-Crick base pairs with cytosine but also Hoogsteen base pairs with adenine<sup>52</sup> see (Figure 2). Mispairing with

adenine gives rise to a GC:TA transversion,<sup>52,53</sup> a frequent mutation of human cancer cells,<sup>52,54</sup> a mutation commonly found in tumor suppressing genes in several hot spot codons of p53 tumor suppressor genes as well as in human Ras proto-oncogenes that are rich in GG sequences.<sup>55</sup>

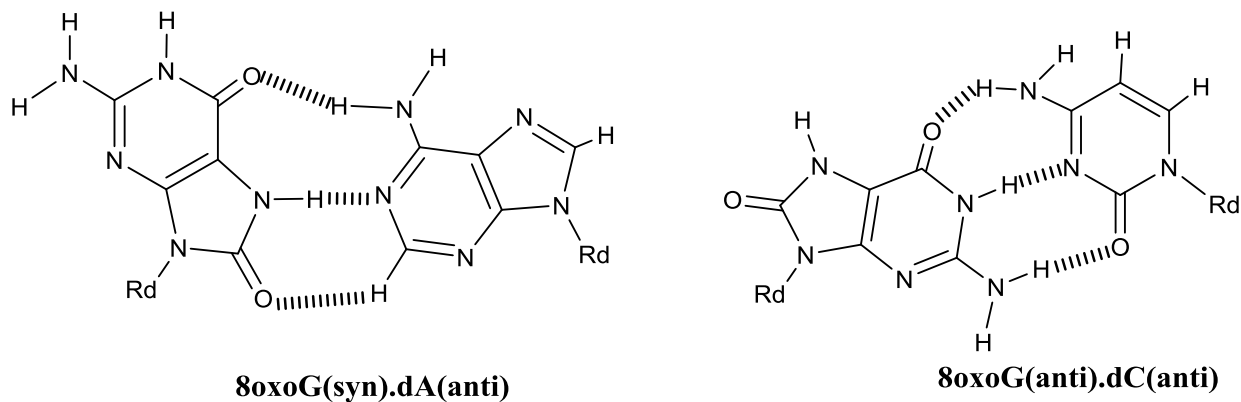


**Figure 2.** 8oxoG pairing with both adenine in the Hoogsteen base pairing and cytosine in the classic Watson-Crick base pair

Because of its low oxidation potential, 8oxoG is susceptible to further oxidation to form a variety of stable products.<sup>32,56</sup> A number of biologically important oxidizers even less potent than  $\bullet\text{OH}$  radicals can oxidize 8oxoG, e.g. carbonate radical  $\text{CO}_3^{\bullet-}$  ( $E^\circ = +1.59 \text{ V}$ )<sup>57</sup> and organic radicals such as alkylhydroperoxyl radical ( $E^\circ = +0.9 \text{ V}$ ).<sup>20</sup> Depending on conditions such as the type of oxidant, pH, and nucleotide environment,<sup>20</sup> 8oxoG is oxidized to form more stable products such as oxaluric acid, produced from oxygen-mediated oxidation of 8oxoG in single stranded DNA.<sup>58</sup> Cyanuric acid and oxaluric acid are produced from peroxy-nitrate-mediated oxidation of 8oxoG in oligonucleotides;<sup>59,60</sup> guanidinohydantion and iminollantoin are produced from 8oxoG in oligonucleotides via oxidation by  $\text{IrCl}_6^{2-}$  that are further oxidized to give parabanic acid and oxaluric acid at pH 7.<sup>61,62</sup> Other products of 8oxoG include

spiroiminodihydantoin,<sup>63</sup> parabanic acid,<sup>64,65</sup> 1,3,5-triazepane-2,4,6,7-tetrone,<sup>66,67</sup> 2,5-diamino-4H-imidazol-4-one,<sup>61</sup> and 2,6-diamino-4-hydroxy-5-formamidopyrimidine, known as FapyG<sup>61</sup> (Figure 3). All these products of 8oxoG oxidation are potential biomarkers of oxidation stress.<sup>33</sup>

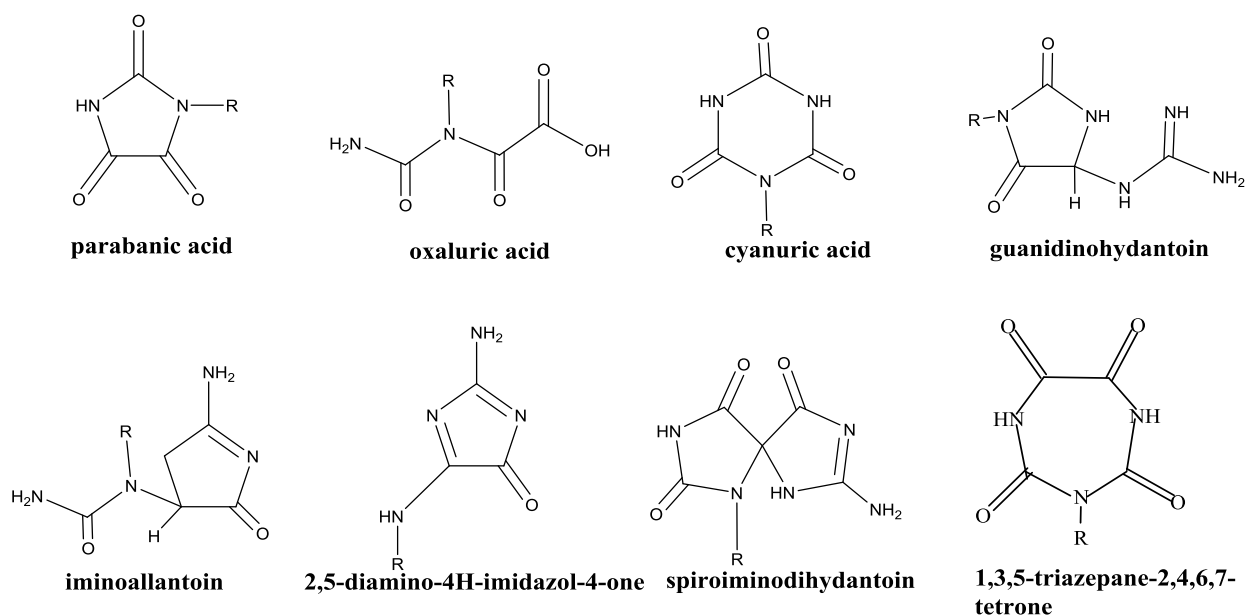


**Figure 3.** Chemical structures of various oxidation products of 8oxoG

8oxoG lesions in DNA can be efficiently removed by enzymatic repair machinery.<sup>4,33,68</sup> The removal of radiation produced DNA lesions by cellular repair process is crucial for reducing levels of mutations and cytotoxicity that are the consequences of failure to repair these lesions. The base excision repair (BER) pathway is the most important and efficient way to remove 8oxoG lesions in DNA along with other oxidized bases.<sup>11,69-72</sup> The repairing process starts by a hydrolytic cleavage of the glycosidic bond between the sugar and the damaged base that is done by the DNA glycosylase to create an abasic site. DNA glycosylase are capable of removing both pyrimidine and purine derivatives lesions.<sup>69</sup> After the removal of the damaged base, repair is

completed by either the short repair path way (one nucleotide gap) or the long repair path way (two to eight nucleotide gap); finally the gap is sealed by DNA ligase.

Following the discovery of 8oxoG in 1984 by Kasai and Nishimura<sup>45</sup> its isolation and analysis were a challenge for many years until 1989 where the first analysis was performed.<sup>73</sup> There were various ways of analyzing 8oxoG, but urine analysis has been found to be the important way of evaluating 8oxoG as a biomarker of oxidative stress.<sup>54,74</sup> Different techniques such as HPLC coupled with electrochemical (HPLC-EC) detection,<sup>54,74,75</sup> GC-MS,<sup>76</sup> and HPLC - mass spectrometry tandem<sup>12,77</sup> have been used to detect and analyze 8oxoG. With time LC-MS was determined to be the most reliable, sensitive, precise, and accurate method as compared to other methods.<sup>45</sup> HPLC with electrochemical detection has been also identified to be a more sensitive and reliable tool than the HPLC-GC-MS<sup>45</sup> that has many drawbacks because of problems associated with increased 8oxoG levels as a result of oxidation during sample preparation.<sup>45</sup>

### Charge Transfer

Charges formed in DNA as a result of DNA oxidation or reduction tend to migrate along the DNA strand from one point to another. Two types of charge transfer in DNA have been identified, namely *hole* and *electron transfer*. Charge migration along the DNA helix has been a center of attention for over 40 years.<sup>78,79</sup> In 1962 Eley and Sprivey<sup>79</sup> proposed the electrical conductivity of DNA. It is now accepted that excess electrons migrate over long distances along the  $\pi$  system of the stacked bases pairs in the double helix of DNA. Understanding the ability of DNA to transfer charges over long distances is very important for prediction and

alleviation of damage to DNA as a result of oxidative stress. Holes are capable of migrating for short or long distances depending on the location of a site with a low reduction potential (hole trap) such as G<sub>n</sub> stretches or 8oxoG.<sup>34,80,81</sup>

Most studies of hole transfer in DNA have been focused on the guanine radical cation. The following experimental strategies have been used to study hole transfer in DNA. Holes in DNA can be initiated photochemically or chemically by using a redox active probe as donors of holes. The process of hole initiation in DNA may be formalized as a point hole injection. The following photoactive donors have been used: 4'-acylated thymidine,<sup>38,82</sup> anthraquinone derivatives,<sup>39,80,83-85</sup> intercalated Rh(III) complex,<sup>39,80,83-85</sup> and riboflavin.<sup>86</sup> Chemically induced probes include intercalated Rh(III) complexes<sup>87,88</sup> and Ni(II) ligands or shift system.<sup>89</sup> The process of the charge transfer from *donor (D)* to *acceptor (A)* in DNA with a known sequence and length (bridge) has been studied by various techniques including measuring the quenching of fluorescence of the donor<sup>90-95</sup> or analysis of relative yields of strand scission at different positions in DNA.<sup>82,83,96,97</sup> Despite the overwhelming number of studies on charge transfer in DNA, the mechanism is still not well understood. Two general mechanisms of charge transfer have been described: a single-step *superexchange* or *tunneling* mechanism for short distance charge transfer (< 10 Å) or a multi-step *hopping* mechanism for long distance charge transfer (> 10 Å) (see Figure 4).

### Superexchange Mechanism

In the superexchange mechanism, the rate of charge transfer,  $k_{CT}$ , depends exponentially on the distance R between the donor and the acceptor. This is described by the Marcus-Levich-Jortner equation:<sup>98</sup>

$$k_{CT}(R) = k_0 \exp(-\beta R) \quad (1)$$

where  $k_0$  is a temperature-dependent pre-exponential factor,  $\beta$  is the falloff parameter that characterizes the steepness of the distance dependence of charge transfer.  $\beta$  depends on the nature of the bridge. Small values of  $\beta$  are typical for materials with high electric conductivity (*weak distance dependence*). The values of  $\beta \sim 0.1 \text{ \AA}^{-1}$  were observed for bridges of conjugated polyenes, likely due to the high extent of delocalization of the donor and acceptor states in the bridge.<sup>78</sup> Materials with low electric conductivity show higher values of the falloff parameter. In this case, the rate of charge transfer strongly depends on the distance. The value of  $\beta \sim 1.7 \text{ \AA}^{-1}$  for electron tunneling in water has been reported.<sup>99</sup> The value of the  $\beta$  falloff parameter for charge transfer in DNA has been a center of huge debate on the processes of charge transport in DNA.<sup>100-104</sup> An enormous amount of work has been done to demonstrate that DNA is actually a semiconductor characterized by a relatively high value of  $\beta$  (the values of the falloff parameter in the range of 0.6 to 1.3  $\text{\AA}^{-1}$  have been reported).<sup>100-104</sup> On the contrary, much lower values of  $\beta$  in DNA have been reported by Barton and co-workers in fluorescence quenching studies<sup>105</sup> and by Schuster and co-workers in photoinduced strand scission studies.<sup>106</sup>

The weak distance dependencies were explained by Barton's group using the concept of the "molecular wire" mechanism.<sup>90</sup> They hypothesized that the donor and acceptor in DNA are strongly coupled to each other through the intervening bridge of  $\pi$  stacks. In this model, DNA was assumed to behave as a molecular conducting wire with a continuous delocalized molecular orbital in which all DNA base pairs are in electronic contact so that charge transfer occurs via the superexchange mechanism. However, it has been demonstrated recently that the hypothesis of a

molecular wire is incorrect.<sup>103,107</sup> Warman et al.<sup>107</sup> argued against one dimensional conductivity in DNA in hydrated irradiated DNA. Debije et al.<sup>103</sup> have demonstrated that DNA at 4 K is a very efficient trap for both holes and electrons, based on high yields of trapped free radicals and the lack of dependence on the length of base stacking in crystalline oligonucleotides.

### Hopping Mechanism

It has been experimentally shown that oxidative damage at G bases can occur as far away from the oxidant as up to 200 Å.<sup>80,83,108</sup> These data seem to be in contradiction with the model of one-step tunneling in which the efficiency of charge transfer is decreased by almost an order of magnitude for every 2 Å. To resolve this contradiction, relatively recently the model of the *hopping mechanism* has been suggested to describe long-distance charge transfer in DNA.<sup>80,83,108,109</sup> According to this model, charges in DNA can migrate via of series a short-distance tunneling processes (hops) from the charge donor, through intermediate shallow traps (Tr), to the charge acceptor (Figure 4B). The hopping mechanism explains why the long-distance charge transport through DNA is possible without considering DNA as a molecular wire. In the mechanism, each hopping step exponentially depends on the hopping distance, in agreement with equation 1, but the total distance of charge transfer is split up into small fractions, so that the distance dependence is no longer one-exponential and is described by a more complex multi-exponential equation.

The hopping mechanism has been experimentally investigated using guanine-rich DNA double stranded oligonucleotides containing a donor site where holes are photochemically generated, guanines as intermediate traps, AT bridges between two guanines, and the GG or GGG unit as a hole acceptor, for example AQ[(A<sub>n</sub>)GG]<sub>n</sub> or AQ[(T)<sub>n</sub>GG]<sub>N</sub>, where n=1 to 7 and



$N=4$ , or  $AQ = AAAGGGAAAGGA AAGGAAAGGAAAGGAAAGG$ , where  $n$  is the number of GG sites  $n=3$  and  $N=6$ .<sup>110</sup> Experiments carried out by Giese et al.<sup>38,55,111</sup> were especially influential. It was found that in double stranded DNA where the  $(AT)_n$  bridges between the guanines are short ( $n < 3$ ), holes hop only between guanines, with the rate of each hopping step strongly depending on the distances between guanines. On the other hand, when the  $(AT)_n$  sequences between the guanines are rather long ( $n > 4$ ), adenines also act as hole intermediate traps.<sup>38</sup>

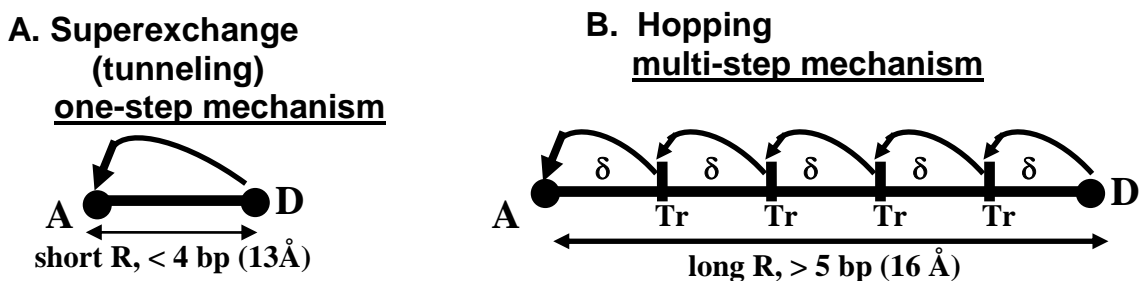


**Figure 4.** Models of charge transfer in DNA: **A.** Superexchange, or tunneling mechanism for short distance charge transfer. **B.** Hopping mechanism for long-distance charge transfer

Previous Models of Long-Distance Charge Migration in DNA

The Diffusion Model of Competitive Electron Scavenging

The *diffusion model* of long-distance charge transfer in DNA was first described by Razskazovskii et al.<sup>112</sup> This group investigated the efficiency of electron trapping in brominated

DNA where the product thymine bromination, 5-bromo-6-hydroxy-5,6-dihydrothymine (T(OH)Br), acted as electron traps. In that work, electron migration was described mathematically using the model of unbiased one-dimensional diffusion under steady state conditions. In this model, electron movement via a trap-to-trap tunneling was assumed to be analogous to a diffusion process. The model is based on the following assumptions:

- The DNA is treated as a one-dimensional array containing equidistant trapping sites C and T or brominated cytosine (Py, shallow electron traps) and T(OH)Br at the terminal of each array serving as a sink (deep electron traps) (Figure 5 and Figure 6)
- Electrons are injected in the DNA array randomly from the bulk with the equal probability anywhere along the strand.
- Migration of electrons through the DNA can be treated as a one-dimensional diffusion. Electrons are capable of diffusing (hopping) from their original site to another with the diffusion constant

$$D = d^2 / 2 \tau_d \quad (2)$$

where  $d$  is the electron transfer hopping distance,  $\tau_d$  is the life time of the electron at one location that can also be represented as  $1/k_d$ , where  $k_d$  is the rate constant of electron diffusion.

- When electrons are injected into the DNA array, they can travel with equal probability in any direction between the shallow traps (unbiased diffusion).
- After one-electron reduction, CBr anion radicals formed as a result of the attachment of the electron to brominated cytosine can undergo reversible protonation with a rate

constant  $k_p$  or a half-life  $\tau_p=1/k_p$ . The reaction of protonation of CBr radical anion competes with the diffusion process of the electron.

- Hopping of electrons can be irreversibly scavenged by T(OH)Br with a rate constant  $k_{sc}$  or a half-life  $\tau_{sc}= 1/k_{sc}$ . In this model only T(OH)Br acts as an irreversible electron scavenger.
- Interstrand electron transfer is considered to be noncompetitive with electrons scavenging within the same strand. The mean separation between the trapping sites in the strand is considered to be equal to the number of bases per trap.

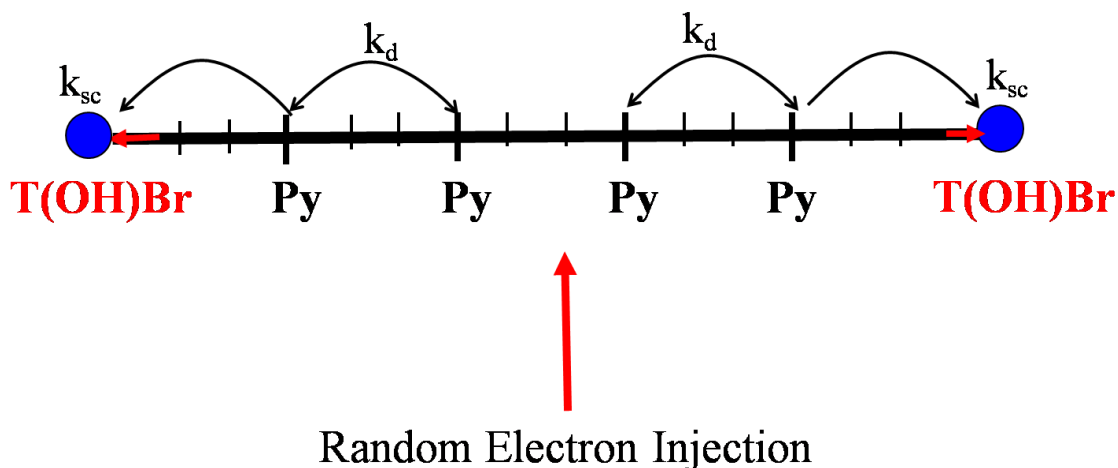


**Figure 5.** Diffusion model of migration of randomly injected electrons in brominated DNA

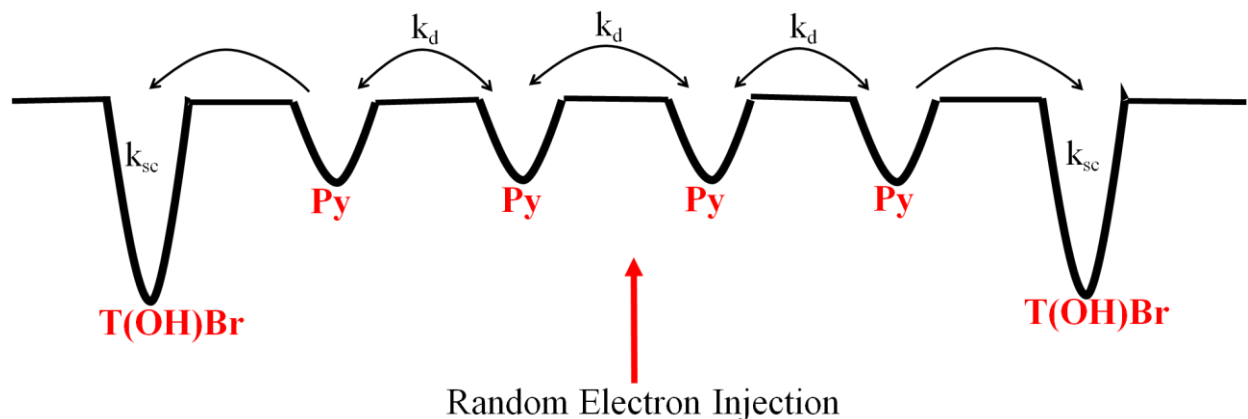


**Figure 6.** Schematic representation of Py sites as shallow electron traps and of T(OH)Br sites as deep electron traps

The solution of steady the state diffusion problem is described in the paper of Razskazovskii et al.<sup>112</sup> The scavenging yield which is the ratio of the number of oxidized scavengers to the total number of electrons injected can be calculated as a function of  $N$  that is the number of bases per dopant atom.

$$R_{sc} = \frac{\beta}{\alpha N(\alpha + \beta \coth(\alpha N))} \quad (3)$$

Where the parameter  $\alpha$  ( $\alpha = \tau_d/2\tau_p = k_p/2k_d$ ) describes the ratio of the rate of two competing processes: CBr protonation and electron diffusion and the parameter  $\beta$  ( $\beta = \tau_d/\tau_{sc} = k_{sc}/k_d$ ) describes the ratio of two other competing processes: electron scavenging at T(OH)Br and electron diffusion. The parameter  $\alpha$  defines the migration process and is also related to the number of diffusion steps the electron makes per protonation event expressed as  $k_d/k_p$ . The parameter  $\beta$  defines the relative efficiency of the diffusion vs. scavenging process. In the system

where electron scavenging occurs much faster than electron diffusion, i.e. under diffusion-controlled regime,  $\beta \coth(\alpha N) \gg \alpha$  and the equation for the scavenging yield (3) can be simplified as

$$R_{sc} = \frac{\tanh(\alpha N)}{\alpha N} \quad (4)$$

### General Principles of the Diffusion Model from Donor to Acceptor

The same basic principles described in Section 1.3.1 were used in a more general solution of the diffusion problem for long-distance charge migration in DNA.<sup>113</sup> In that work, which focuses on a more experimentally relevant situation of a *point charge injection* rather than on a *random charge injection*, an analytical solution has been described for both the time-dependent problem and steady state problem of charge transfer through a DNA bridge via hopping mechanism. In this model, which focuses on hole transfer in DNA, DNA is considered as a one-dimensional array with  $N$  equidistant traps of guanine. The distance between traps is  $\delta$  so the total length of the bridge is  $L = \delta N$ . At each end of the array there are a donor that serves as a point hole injector and an acceptor that irreversibly scavenges these holes (see Figure 7 and Figure 8). The progress of charge migration is monitored by the yield of oxidized acceptor  $A_{ox}$  or by the yield of oxidation of intermediate trapping sites (single guanines). The same three rate constants as in the previous section are used to describe the process of hole migration and trapping: the rate constant of diffusion,  $k_d$ , the rate constant of reaction,  $k_r$ , and the rate constant of scavenging,  $k_{sc}$ .

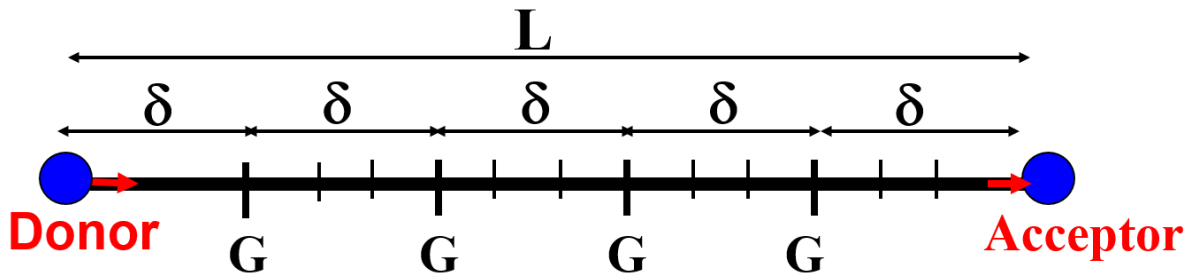


**Figure 7.** The diffusion model of charge migration from the donor to the acceptor

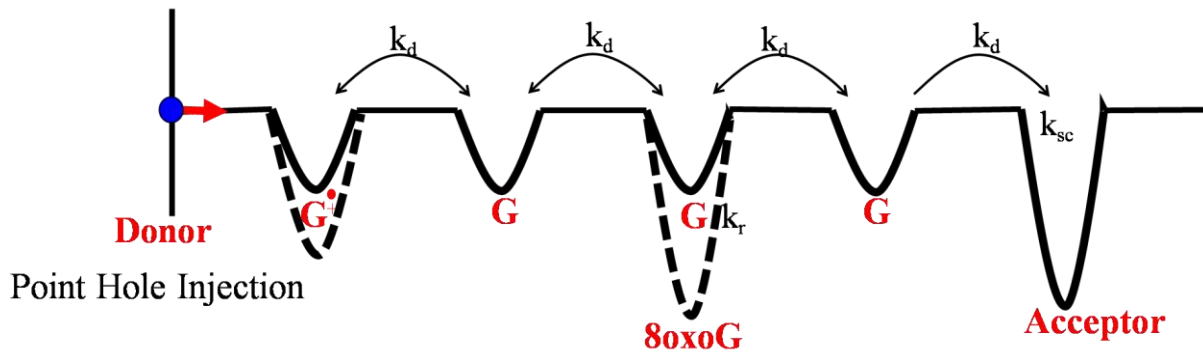


**Figure 8.** Schematic representation of G sites as shallow hole traps and of the acceptor site as a deep hole trap

The model uses the same basic assumptions described in Section 1.3.1. To analytically describe the concept of the donor as a point hole injector and the acceptor as an irreversible sink for the hole, the following additional assumptions were used:

- The hole is injected into the DNA array by the donor D at  $x=0$  instantly and irreversibly. This means that once the hole is injected into the array it never returns to the strand ('the mirror' approximation).

- Upon reaching the boundary of the acceptor A, the hole can either be reflected from its boundary or irreversibly trapped by the relaxation of trapping ('the grey sphere' approximation).

The diffusion process compete by an irreversible chemical transformation of the hole characterized by the cumulative rate constant  $k_r$ . Analytical solution for the steady state problem of hole diffusion in DNA gave the following Equation (5):

$$R_{sc} = \frac{\omega}{\alpha \sinh(\alpha N) + \omega \cosh(\alpha N)} \quad (5)$$

where  $\omega = 2k_{sc}/k_d$ ,  $\alpha = (2k_r/k_d)^{1/2}$ . For diffusion-controlled regime  $k_{sc} \gg \gg k_d$ , so  $\omega \rightarrow \infty$  and Equation (5) is reduced to Equation (6):

$$R_{sc} = \frac{1}{\cosh(\alpha N)} = \text{sech}(\alpha N) \quad (6)$$

### Specific Aims

The long-term goal of this study was to quantitatively characterize the kinetics of 8oxoG formation and disappearance in DNA as a result of DNA oxidative damage using the diffusion model of hole migration in DNA. The accumulation of 8oxoG in highly polymerized DNA, oxidized by  $\text{Br}_2^\bullet$  resulting in the steady state concentration of one 8oxoG per  $127 \pm 6\text{pb}$  has been established.<sup>30</sup> 8oxoG can be produced only at these low levels because of its further oxidation to other species.<sup>30</sup> Cai and Sevilla<sup>30</sup> made assumptions on the 'second hit event' which eventually lead to the disappearance of 8oxoG as it oxidizes mobile holes in DNA. However, this

phenomena has not yet been characterized quantitatively in terms of mobility in DNA and has never been investigated using other oxidants. Research group of Shafirovich<sup>114,115</sup> have shown by product analysis that indeed 8oxoG is further oxidized using the carbonate radical anion as an oxidant. No analysis has been performed to show how efficient this process is, and whether it is related to hole mobility in DNA.

The specific aims of the present work are stated below:

- 1) To compare the efficiency of 8oxoG production in DNA by various oxidants such as  $\text{Br}_2^\bullet$ ,  $\text{SO}_4^\bullet$ ,  $\bullet\text{OH}$ ,  $\text{CO}_3^\bullet$ ,  $\text{SeO}_3^\bullet$  and  $(\text{SCN})_2^\bullet$ . Although these species have different oxidation potential and mechanism of DNA oxidation that might affect the initial accumulation, the steady state concentration of the 8oxoG is expected to be independent of the type of oxidant and only to depend on the of parameters of the hole migration as well as DNA composition and structure.
- 2) To verify the assumption that formation of 8oxoG in DNA involves long-distance hole migration. The kinetics of 8oxoG accumulation and disappearance will be studied for different types of polymeric DNA with various structures and the CG content. The steady-state concentration of 8oxoG is supposed to be dependent on both DNA composition and structure. We hypothesize that the number of 8oxoG formed per DNA base pair will decrease with the increase of the CG content in DNA because of the increased probability of hole migration and as the result of the increased frequency of the 'second hit' events due to a higher number of guanines as intermediate traps.



**3)** To extract characteristics of hole mobility in DNA from the experimental data on kinetics of 8oxoG formed as a result of oxidative damage to DNA, such as the ratio of the rate constant of hole oxidation,  $k_r$ , and the rate constant of hole transfer in DNA,  $k_d$ . Experimental results were analyzed using a diffusion model of charge migration in DNA that treats hole migration as a one-dimensional diffusion.

## CHAPTER 2

### RATIONALE AND APPROACHES

#### 8oxoG Production by Various Oxidants

Bases are the most oxidizable components of DNA. Guanine has the lowest reduction potential of +1.29 V,<sup>57</sup> while adenine (A), Cytosine (C), and thymine (T) are characterized by much higher reduction potentials: +1.56 V, +1.6 V, and +1.7 V, respectively.<sup>24</sup> A list of potential oxidizers is summarized in Table 1. The choice of potential oxidants of G (hole injectors) for the present research was based on the following factors:

- The reduction potential of oxidizing species chosen should be higher than that of guanine, i.e. higher than +1.29 V, a list of the standard reduction potentials of DNA bases in nucleosides is summarized in Table 2;
- It should be easy to generate the oxidizing species using available methods;
- A given oxidizing species must be relatively stable;
- A given oxidizing species must be active in the range of physiological pH. Thus, though the dichloride radical anion,  $\text{Cl}_2^{\bullet-}$ , is characterized with a suitable reduction potential of +2.3 V, it is formed only at basic pH.<sup>21</sup>

**Table 1.** Standard reduction potentials of inorganic radicals<sup>21</sup>

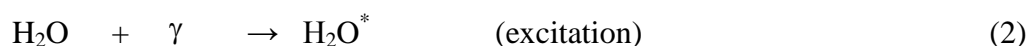
Couple	Standard Reduction Potential (E°/V)
$\bullet\text{OH}, \text{H}^+/\text{OH}^-$	+2.73
$\text{SO}_4\bullet^-/\text{SO}_4^{2-}$	+2.47
$\text{SeO}_3\bullet^-/\text{SeO}_3^{2-}$	+1.77
$\text{Br}_2\bullet^-/2\text{Br}^-$	+1.60
$\text{CO}_3\bullet^-/\text{CO}_3^{2-}$	+1.59
$(\text{SCN})_2\bullet^-/2\text{SCN}^-$	+1.33

**Table 2.** Standard reduction potentials of DNA bases in nucleosides<sup>24,27</sup>

Name of Base	Standard Reduction Potential (E°/V)
Thymine	+1.70
Cytosine	+1.60
Adenine	+1.56
Guanine	+1.29

## Hydroxyl Radical ( $\bullet\text{OH}$ )

The  $\bullet\text{OH}$  radical is the most versatile and the most powerful of all oxidants under consideration (the reduction potential of the couple  $\bullet\text{OH}, \text{H}^+/\text{H}_2\text{O}$  is  $= +2.73 \text{ V}$ .<sup>57</sup> It is generated via radiolysis of water that is initiated by the ionization or excitation of water (the symbol  $\gamma$  represents ionizing radiation):<sup>21</sup>



An excited or ionized water molecule undergoes further reactions with production of the hydroxyl radical:



Depending on the pH of the solution,  $\bullet\text{OH}$  can be a very potent oxidant with a standard reduction potential of  $+2.73\text{V}$ <sup>57</sup> in acidic or neutral solutions. Three major reaction types of  $\bullet\text{OH}$  have been identified.<sup>21</sup> These are: addition to double bonds, hydrogen abstraction, and electron transfer. Double bond addition is the most preferred reaction path of  $\bullet\text{OH}$  because of its electrophilic nature that  $\bullet\text{OH}$  makes it regioselective, reacting with the most electron-rich site in the substrate.

### Dibromide Radical Anion ( $\text{Br}_2^{\bullet-}$ )

$\text{Br}_2^{\bullet-}$  is one of the most selective and powerful oxidant of guanine. The standard reduction potential of  $\text{Br}_2^{\bullet-}$  is (+1.60 V).<sup>57</sup> It is quickly generated in irradiated aqueous solutions of bromide salts by initially forming a three-electron bond adduct radical with a nearly diffusion-controlled rate constant ( $k = 1.1 \times 10^{10} \text{ M}^{-1} \text{ s}^{-1}$  (Reaction 5)).<sup>27</sup> There is further decomposition of the adduct to form  $\text{OH}^-$  and  $\text{Br}^\bullet$  ( $k = 4.2 \times 10^6 \text{ s}^{-1}$  (Reaction 6))<sup>21</sup> that is the rate determining step.  $\text{Br}^\bullet$  then reacts with another bromide anion to form a weak  $\sigma$ - $\sigma$  three-electron bond in an equilibrium reaction resulting in  $\text{Br}_2^{\bullet-}$  ( $K=10^{10} \text{ M}^{-1} \text{ s}^{-1}$ ) ( reaction 7)<sup>21</sup> and equilibrium constant of  $\text{Br}_2^{\bullet-}$  to be  $3.9 \times 10^5$ .<sup>84</sup>



$\text{Br}_2^{\bullet-}$  is known to react exclusively by outer sphere electron transfer. The selective nature of  $\text{Br}_2^{\bullet-}$  makes it a convenient source of holes in the DNA. Because Reaction (5) is very fast and the constant of formation of  $\text{Br}_2^{\bullet-}$  is quite large, hydroxyl radicals produced during radiolysis of water are nearly quantitatively converted into  $\text{Br}_2^{\bullet-}$  so that the radiation chemical yield of  $\text{Br}_2^{\bullet-}$  is very close to that of  $\bullet\text{OH}$ .

### Sulfate Radical Anion (SO<sub>4</sub><sup>•-</sup>)

Sulfate radical anion can be generated from the persulfate anion, S<sub>2</sub>O<sub>8</sub><sup>2-</sup>, photolytically using a UV light (Reaction 8)<sup>21</sup>. It can also be generated by reduction of persulfate anion by e<sup>-</sup><sub>(aq)</sub> (k= 1.2 x 10<sup>10</sup> M<sup>-1</sup>s<sup>-1</sup> (Reaction 9)) and H<sup>•</sup> (k= 1.4 x 10<sup>7</sup> M<sup>-1</sup>s<sup>-1</sup> (Reaction 10))<sup>21</sup> during radiolysis of aqueous solutions of persulfate salts.



Sulfate radical anion is the second strongest oxidant generated in neutral solutions with a standard reduction potential of +2.60 V.<sup>21</sup> Owing to this high reduction potential, SO<sub>4</sub><sup>•-</sup> reacts with all DNA bases indiscriminately, similar to the hydroxyl radical. The mechanism of reaction with DNA is similar to <sup>•</sup>OH; sulfate radical anion is electrophilic in nature and preferably adds to the electron-rich position of a substrate.

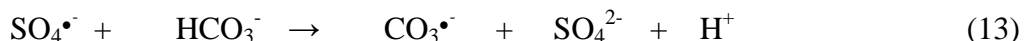
### Carbonate Radical Anion (CO<sub>3</sub><sup>•-</sup>)

With the standard reduction potential of +1.59 V, which is similar to that of Br<sub>2</sub><sup>•-</sup>, CO<sub>3</sub><sup>•-</sup> is known to selectively react with guanine.<sup>56</sup> It can be generated by different methods. Carbonate radical anions can be produced by one-electron oxidation of CO<sub>3</sub><sup>2-</sup> or HCO<sub>3</sub><sup>-</sup> by <sup>•</sup>OH, with rate constants k = 3.9 x 10<sup>8</sup> M<sup>-1</sup> s<sup>-1</sup> (reaction 11)<sup>21</sup> and k = 8.5 x 10<sup>6</sup> M<sup>-1</sup> s<sup>-1</sup> (reaction 12),<sup>21</sup> respectively.



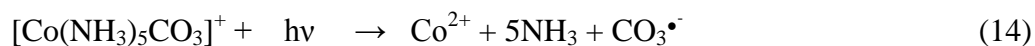


$\text{CO}_3^{\bullet-}$  can be also generated via the reaction between  $\text{SO}_4^{\bullet-}$  and bicarbonate anion in irradiated aqueous solutions of persulfate and bicarbonate:<sup>21</sup>



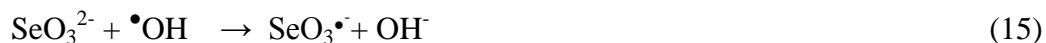
Another way of generating  $\text{CO}_3^{\bullet-}$  is by UV photolysis of aqueous solutions of carbonatopentamminecobalt (III) or carbonatotetramminecobalt (III) complexes,<sup>115</sup> e.g.

$[\text{Co}(\text{NH}_3)_5\text{CO}_3]^+$ :

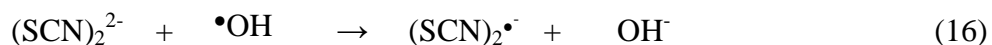


### Other Oxidants

Selenite Radical Anion  $\text{SeO}_3^{\bullet-}$  Selenite radical anion has a considerably high redox potential (+1.77 V)<sup>57</sup> in neutral solutions and is typically generated by reacting of the selenite anion  $\text{SeO}_3^{2-}$  with  $\bullet\text{OH}$  during radiolysis of aqueous solutions of selenite salt.  $\text{SeO}_3^{\bullet-}$  is known to oxidize specifically at the guanine sites<sup>116-118</sup> with a rate constant of  $3 \times 10^7 \text{ M}^{-1}\text{s}^{-1}$ .<sup>117,118</sup>



Thiocyanate radical anion (SCN)<sub>2</sub><sup>•-</sup> Thiocyanate radical anion has a redox potential of +1.33V<sup>57</sup> and can be generated from thiocyanate ion (SCN)<sub>2</sub><sup>2-</sup> (Reaction 16). Its standard reduction potential is only slightly higher than guanine but still this species might have the potential to oxidize guanine in DNA.



### The Effect of DNA Structure and G Content on 8oxoG Production

The kinetics of 8oxoG formation and disappearance was studied using native DNAs with different CG content such as salmon testes DNA (42% of CG) or micrococcal DNA (71.9% of CG) or synthetic polymeric DNAs with different CG content or sequence such as poly(deoxyguanylic-deoxycytidylic) acid sodium salt poly(CG-GC), poly(deoxyguanylic)-poly(deoxycytidylic) acid sodium salt poly(GG-CC) (both have 100% CG but different sequence of C and G). This relatively short list of different types of DNA we studied is related to the very high price of synthetic DNAs and a very limited number of DNAs with different sequences in the market. In future projects, RNAs with different sequences and CG content might be used instead of DNAs because of much higher availability and much lower prices.

The steady state yields of 8oxoG were compared for DNA with different CG content to test the hypothesis that the increase in CG content causes the decrease in the steady state concentration of 8oxoG and for DNA with the same CG content but different sequences, such as poly(CG-CG) and poly(GG-CC). In the poly(CG-GC) homopolymer that contains two self-complementary strands, two types of hole hopping between two guanines are possible (see Figure



9): an intrastrand hopping between two guanines located on the same strand and separated by cytosine and an interstrand hopping between neighboring guanine located on opposite strands. In the poly(GG-CC) heteropolymer, the only possibility for the hole migration is by hopping between neighboring guanines (Figure 10).

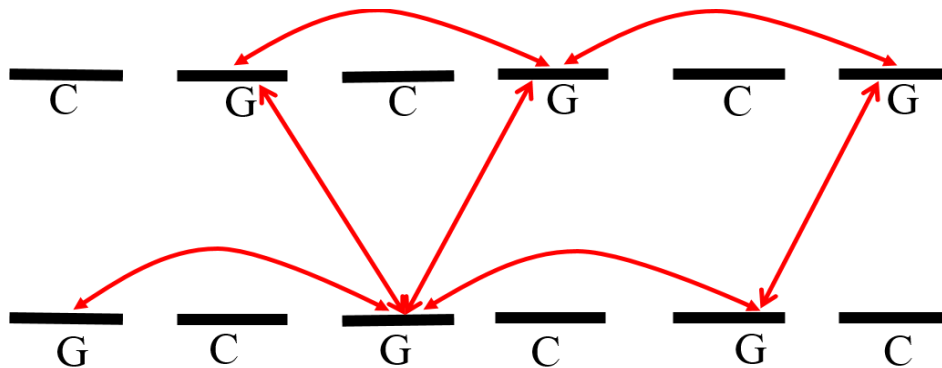


**Figure 9.** An intrastrand hopping between guanines located on the same strand separated by cytosine and an interstrand zig-zag hopping between guanines located on opposite strands in poly(CG-GC)

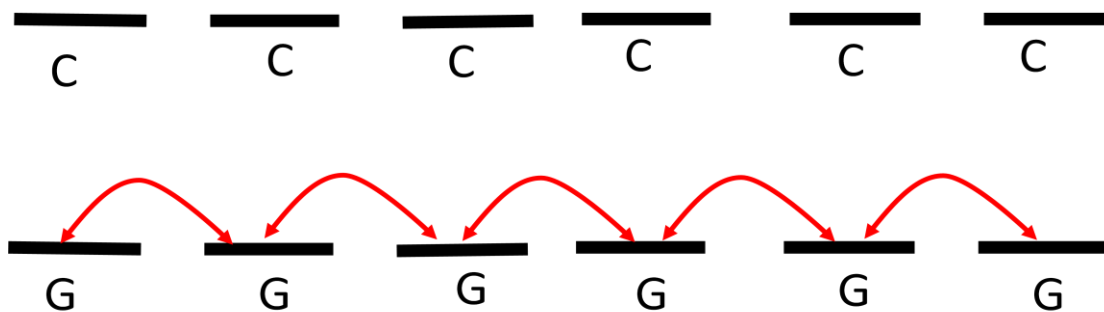


**Figure 10.** An intrastrand hopping between guanine located on the same strand in poly(GG-CC)

Analysis of Experimental Data on 8oxoG Kinetics Using the Diffusion Model of Hole Transfer  
in DNA

The 8oxoG kinetic experimental data were mathematically treated using the diffusion model of charge migration in DNA, an approach analogous to that described in the previous works of our research group Razskazovskii et al.<sup>112</sup> and in Roginskaya et al.<sup>113</sup>.

General Principles of the Diffusion Model of 8oxoG Kinetics

The assumptions of the diffusion model (Figure 11) and Figure 12 shows the energetic traps of hole:

- DNA is treated as a one-dimensional array with a length  $L$  of equally spaced guanines as trapping sites;  $\delta$  is the distance between guanines, with 8oxoG at each end of the array, so the number of guanine traps in the array is  $L/\delta$ .

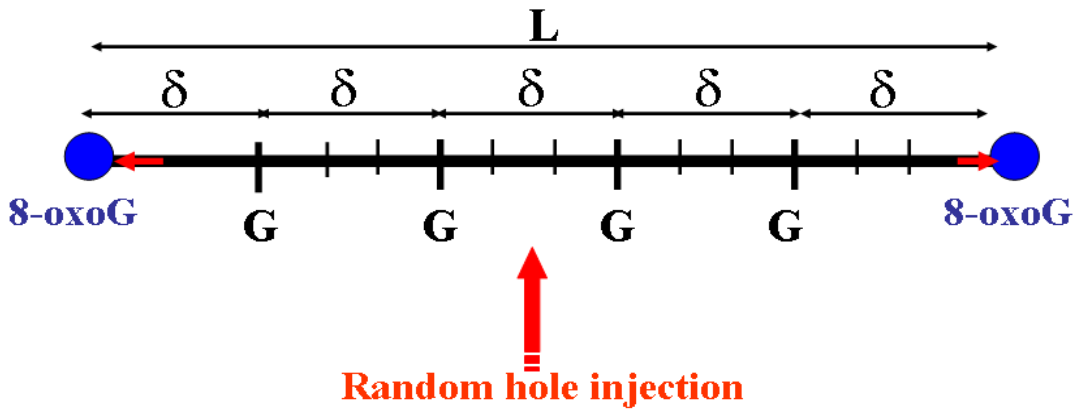


**Figure 11.** The diffusion model of the hole transfer describing the formation and oxidation of 8oxoG in the DNA.  $\delta$  is the distance between G;  $L$  is the average distance between neighboring 8oxoG;  $L=N_{\text{bases}}/\delta$ .

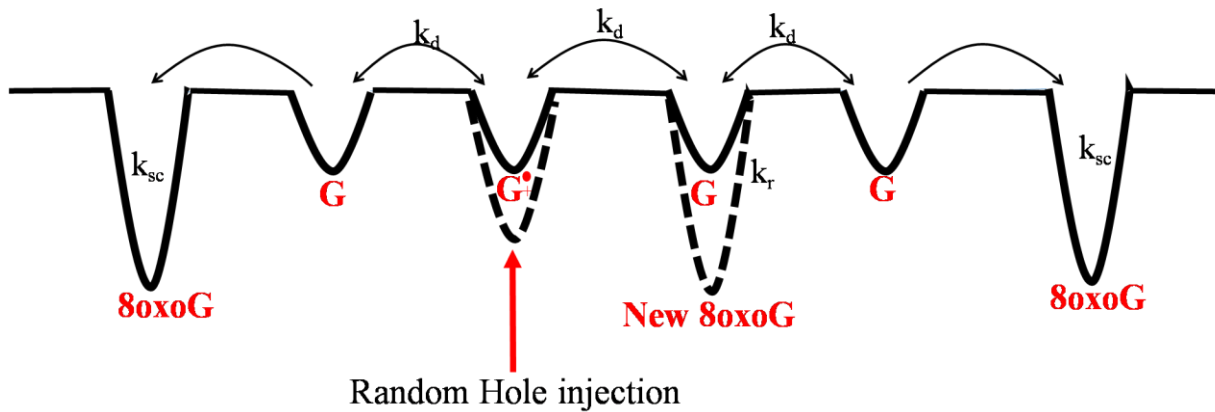
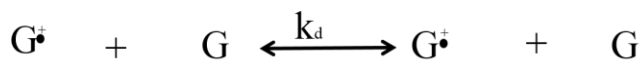
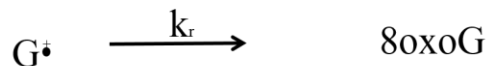


**Figure 12.** Schematic representation of G sites shown as shallow hole traps and 8oxoG sites as deep electron traps

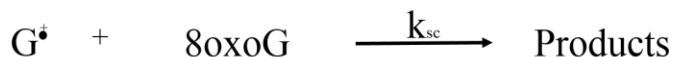
- Holes are randomly injected into the array anywhere with equal probability.
- Hole injection from the bulk into the DNA array occurs irreversibly because the reduction potential of an oxidizing species from the bulk (hole injector) is much higher than the oxidizing potentials of guanine.
- Hole migration between two neighboring guanines occurs by the tunneling mechanism and is mathematically described by the Marcus-Levich-Jortner equation  $k_{ht} = e^{-\beta r}$ , where  $k_{ht}$  is a rate constant of hole transfer,  $\beta$  is a 'falloff' parameter, and  $r$  is the distance of hole transfer.
- Formation of 8oxoG creates a deep irreversible hole trap because the reduction potential of 8oxoG, 0.74 V,<sup>22</sup> is much lower than the reduction potential of guanine, 1.29 V.<sup>22</sup>
- As a result, an array of 8oxoG separated by guanines is formed. The mean distance between 8oxoG in terms of the number of diffusion steps  $N$  is:  $N = (\text{Total concentration of G}) / (\text{Concentration of 8oxoG}) = [G] / [8oxoG]$ .
- 8oxoG is oxidized if a hole injected between two 8oxoG reaches one of them by hopping along guanines as intermediate traps.
- A hole injected into this DNA array has two possible fates: a) to reach one of the ends of the array and further oxidize 8oxoG or b) to react with one of guanines in the array to form a new 8oxoG. In both cases, a present array will disappear and a new array of the same type will be formed.
- The processes occurring in this system can be described by the following kinetic scheme:



Hole hopping



Reaction of  $G^{\bullet}$  to form 8oxoG



Hole scavenging at 8oxoG to form products

**Scheme 1.** Kinetic scheme of the diffusion model where  $k_d$  is the rate constant of hole diffusion (hopping),  $k_r$  is the rate constant of 8oxoG formation, and  $k_{sc}$  is the rate constant of hole scavenging by 8oxoG, i.e. the rate of 8oxoG oxidation. Under the reasonable assumption that the scavenging of holes by terminal 8oxoG occurs much faster than hole diffusion ( $k_{sc} \gg k_d$ ),  $k_{sc}$  will not appear in the final kinetic equation.

### Mathematical Approach

The *scavenging yield of 8oxoG*,  $R_{sc}$ , is defined as the ratio of the number of 8oxoG produced in a DNA array to the total number of hole injected into this array. The scavenging yield can be also represented as the probability  $P$  of the event that a hole in an array will reach one of the ends of the array to be trapped by 8oxoG;  $P = \tanh(\alpha N)/\alpha N$  where  $\alpha = (k_r/2k_d)^{1/2}$ , as derived in Razskazovskii et al.<sup>112</sup> As previously mentioned, the hole in the DNA array has only two fates: to be irreversibly trapped by 8oxoG at either end of the array to oxidize 8oxoG and

thus to destroy a given array or to be trapped by any G in the array to form a new 8oxoG and thus to create a new array. Then the probability that the hole will be trapped as a new 8oxoG is  $1-P$ . The net probability that a new 8oxoG will be formed can be calculated at the difference of probabilities of formation of a new 8oxoG and of destruction of an 'old' 8oxoG at the end:

$$(1-P)-P = 1-2P \quad (6)$$

The equation for dose dependence of 8oxoG accumulation can be derived based on the following considerations. The rate of [8oxoG] change can be described as:

$$\frac{d[8oxoG]}{dt} = I_h \Gamma (1-2P) \quad (7)$$

where  $I_h$  is the *intensity of hole injection* and  $\Gamma$  is the *radiation chemical yield of hole formation*.

This equation can be modified by dividing both parts of the equation over  $I_h$  and keeping in mind that the dose D is equal to the product of intensity and time:  $D = I_h t$  and so  $dD = I_h dt$ . Then the dose dependence for 8oxoG can be expressed as following:

$$\frac{d[8oxoG]}{dD} = \Gamma (1-2P) \quad (8)$$

Because  $[8oxoG] = [G]/N$ ,  $d[8oxoG] = -[G]dN/N^2$  then the final equation takes the form

$$\frac{dN}{dD} = -\frac{\Gamma N^2}{[G]} \left(1 - \frac{2 \tanh(\alpha N)}{\alpha N}\right) \quad (9)$$

or by expressing  $X = 1/N = [8\text{oxoG}]/[G]$ :

$$\frac{dX}{dD} = -\frac{\Gamma}{[G]} \left(1 - \frac{2 X \tanh(\alpha/X)}{\alpha}\right) \quad (10)$$

For low doses when very little of 8-oxoG is produced, X is small,  $\alpha/X$  is very large, and  $\tanh(\alpha/X) \approx 1$  and, therefore, P is close to zero, which means that the  $R_{sc}$  value is very low.

Therefore, for low doses we can approximate eq. 8 by:

$$\frac{dX}{dD} = \frac{\Gamma}{[G]} \quad (11)$$

that shows linear accumulation of 8oxoG and allows for direct determination of  $\Gamma$ . To model the entire curve the parameter  $\alpha$  is needed as well. It can be obtained from the steady-state concentration of 8oxoG. When this state is reached,  $dX/dD = 0$  and eq. 8 turns into:

$$1 - \frac{2 X_{\infty} \tanh(\alpha/X_{\infty})}{\alpha} = 0 \quad (12)$$

where  $X_{\infty}$  is the ratio of [8oxoG] to [G] for the steady state concentration of [8oxoG]. The transcendent equation 12 can be solved graphically where  $y = 1 - 2 \tanh(x)/x$ ;  $x = \alpha / X_{\infty}$  and has a solution at  $\alpha/X_{\infty} = 1.915$  (Figure 13). So  $\alpha = 1.915 X_{\infty}$ . Because  $\alpha = (k_r/2k_d)^{1/2}$ , we obtain the

expression for the  $k_r/k_d$  ratio as:

$$k_r/k_d = 7.33 (X_\infty)^2 \quad (13)$$

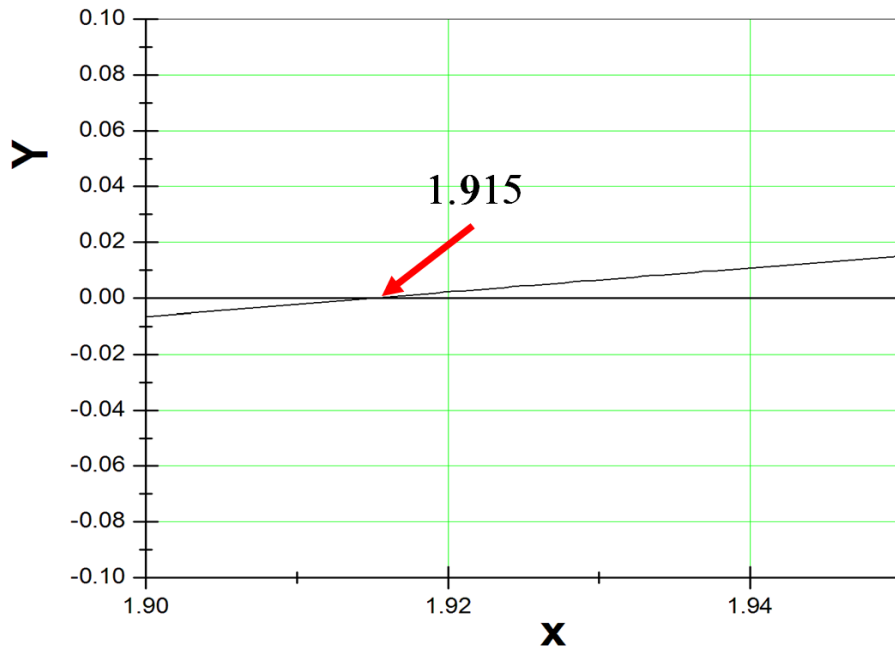


**Figure 13.** Graphical solution of Equation 12, where  $y = 1-2\tanh(x)/x$ ;  $x = \alpha/ X_\infty$



## CHAPTER 3

### EXPERIMENTAL METHODS

#### Instrumentation, Glassware and Other Materials

##### Instrumentation

A Prominence High Performance Liquid Chromatograph (from Shimadzu) supplied with an autosampler, degasser, column oven, and a photodiode array (PDA) detector was used as a major research instrument for product separation and analysis. A Cary 100 Bio UV-Visible Spectrophotometer (from Agilent) was used for determining concentration of samples and for sample analysis. A Philips X-ray tube with a tungsten anode was employed as a source of radiation. A high pressure Xe(Hg) lamp was used as a source of UV light for photolysis. A vacuum set made up of Labconco Centrivap Concentrator, Labconco Rotary Vane Electric Pump, and a pressure gauge was used for sample concentrating or degassing by the freeze-pump-thaw method. Other instrumentation used in the present research included a pH meter, laboratory balances, oven, water bath, vortex mixer (all from Fisher Scientific).

##### Glassware and Other Materials

Other important glassware and materials such as beakers, volumetric flasks, measuring cylinders, pasture pipettes, glass vials, Wheaton ampoules, graduated pipettes, pipette tips, disposal pipettes, graduated mixed plastic tubes 1.5mL/0.5mL, centrifuge tubes 50mL/15mL, and magnetic stirrers were employed throughout the experiments.

## Reagents Grade Stock Chemicals

### Deoxyribonucleic Acids and Nucleobases

Highly polymerized salmon testes DNA sodium salt, highly polymerized DNA from *Micrococcus luteus* (*lysodeikticus*) (micrococcal DNA), poly(deoxyguanylic)-poly(deoxycytidylic) (poly(GG-CC)), and poly(deoxyguanylic-deoxycytidylic) (poly(CG-GC)) were purchased from Sigma-Aldrich Chemical Co., DNA nucleobases were all purchased from Sigma-Aldrich Chemical Co. 8oxoG was a generous gift Dr. Steven Swarts (Department of Radiation Oncology, University of Florida).

### HPLC Solvents

HPLC-grade acetonitrile ( $\text{CH}_3\text{COCN}$ ) (from VWR) and HPLC-grade water (Fisher) were used for preparation HPLC solvents. Ammonium acetate (ACS grade from Fisher) was used for preparation of an aqueous mobile phase.

### Buffers, Solutions, and Gases

HPLC-grade water was used for preparation of all stock solutions. One M stock solutions of potassium dibasic phosphate  $\text{K}_2\text{HPO}_4$  and potassium monobasic phosphate  $\text{KH}_2\text{PO}_4$  (both from Sigma) were mixed in a 1:1 ratio to make a 1 M phosphate buffer, pH 6.9, which was diluted to 10 mM phosphate buffer, pH 6.9 for DNA sample preparations. One M perchloric acid (from Fisher) was used for adjusting pH; 1 M sodium hydroxide solution (from Fisher) was used to dissolve 8oxoG; 88% aqueous solution of formic acid  $\text{HCOOH}$  (from Sigma) was used for DNA hydrolysis, isopropanol (from Fisher) was used in a centrifuge cold trap, liquid nitrogen

was used to freeze sample for the freeze-pump-thaw cycle, oxygen (gas) was used for the oxygen-air flame for the glasswork. Both liquid nitrogen and oxygen were supplied by the local Airgas Company.

### Other Reagents Used

Carbonatopentamminecobalt (III) complexes (e.g.  $[\text{Co(III)(NH}_3)_5\text{CO}_3]\text{ClO}_4$ ) were synthesized in our lab according to Martin et al.<sup>119</sup> and used as a photolytic source of  $\text{CO}_3^{\bullet-}$  radical anions. All other reagents and solvents used were of the highest available grade from either Sigma-Aldrich Chemical Co. or Fisher Scientific Co. Potassium persulfate ( $\text{K}_2\text{S}_2\text{O}_8$ ), sodium bromide ( $\text{NaBr}$ ), and sodium bicarbonate ( $\text{NaHCO}_3$ ) were used in experiments with different DNA hole injectors. Potassium persulfate was used to generate  $\text{SO}_4^{\bullet-}$  radical anions during UV photolysis or, together with sodium bicarbonate, to generate  $\text{CO}_3^{\bullet-}$  by radiolysis; sodium bromide was used to produce  $\text{Br}_2^{\bullet-}$  radical anions by radiolysis. Protamine and spermine hydrochloride were used to precipitate DNA. Ferrous (II) sulfate ( $\text{FeSO}_4$ ), sodium chloride ( $\text{NaCl}$ ), and  $\text{H}_2\text{SO}_4$  were used for Fricke dosimetry.

## Experimental Procedures

### Samples Preparation

Preparation of DNA solutions. Ten mM (here and later in the text DNA concentration is expressed in DNA nucleotides) DNA stock solution was routinely prepared by dissolving 36 mg salmon testes DNA salt in 10 mL of 10 mM phosphate buffer, pH 6.9, stored at 4°C overnight to

let the DNA soak, and on the next day the DNA solution was homogenized by gentle stirring. The stock solution was stored at 4°C.

For the experiment that included generation of carbonate radical anions by radiolysis, 10mM salmon testes DNA salt was prepared by dissolving 36 mg salmon tests DNA in 30mL of 340mM sodium bicarbonate. The pH was then adjusted to 7.4 with 1 M NaH<sub>2</sub>PO<sub>4</sub>. After equilibrating overnight at room temperature, the pH was again readjusted to 7.4 and stored at 4°C. Micrococcus Luteus DNA was prepared by dissolving 260 mg in 3.92 mL 10 mM phosphate buffer, pH 6.9. One mM solution of poly (CG-GC) was prepared by dissolving 10 optical units in 1.52 mL of 10 mM phosphate buffer, pH 6.9. Ten optical units of poly (CC-GG) was dissolved in 1.00 mL of 10 mM phosphate buffer, pH 6.9 to produce 0.72 mM.

Preparation of Stock Solutions. A saturated solution of 8oxoG was prepared by dissolving of a small amount of 8oxoG in 100 µL of 100 mM NaOH and further diluted with 900 µL of 40 mM ammonium acetate pH 6.9 and was left overnight at room temperature. Addition of NaOH was necessary to dissolve 8oxoG, which is poorly soluble at neutral pH. The clear solution was separated from the precipitate and stored for future use at room temperature for several days. It has been verified experimentally that the stock solution of is 8oxoG is stable under these conditions. Three hundred forty mM solution of NaHCO<sub>3</sub> was prepared by dissolving 1.428 g in 50 mL distilled water. One hundred mM solution of K<sub>2</sub>S<sub>2</sub>O<sub>8</sub> was prepared by dissolving 0.2703 g in 10 mL distilled water. One M solution of NaBr was prepared by dissolving 1.0289 g in 5 mL distilled water. One M solution of NaOH was prepared by dissolving 4.01 g in 100 mL distilled water. From this stock solution 1 mL aliquot was taken to prepare a 100 mM solution. Four M solution ammonium acetate was prepared by dissolving 154

g of ammonium acetate in 500 mL HPLC grade water. From this stock solution, 40 mM ammonium acetate was prepared for the HPLC aqueous mobile phase and stored at 4 °C. Eighty % acetonitrile as the HPLC organic mobile phase was made by mixing 4 volumes of pure HPLC grade acetonitrile with 1 volume of HPLC grade water.

#### Determination of the Extinction Coefficient of 8oxoG at 305nm

The choice of wavelength of 305 nm for detection of 8oxoG was based on the comparison of the UV-Vis spectra of 8oxoG and G (see Chapter 4). Various dilutions of 8oxoG were prepared (1x, 0.8x, 0.6x, 0.4x, and 0.2x; where 1x designates the concentration of the original saturated solution) and quantified spectrophotometrically at absorbance of 305nm and 285nm (extinction coefficient of 8oxoG was reported at 285 nm).<sup>120</sup> A linear regression of absorbance at 285nm versus 305nm was plotted to determine the slope that was used for calculation of the extinction coefficient of 8oxoG at 305 nm.

#### Fricke Dosimetry

Fricke dosimetry is useful in converting irradiation times into doses. It is chemically based on the conversion of  $\text{Fe}^{2+}$  into  $\text{Fe}^{3+}$ .  $\text{Fe}^{2+}$  is oxidized into  $\text{Fe}^{3+}$  as a result of radiolysis of aqueous solutions of  $\text{Fe}^{2+}$ ;  $\text{Fe}^{3+}$  has a characteristic absorption spectrum with the maximum at 304 nm;  $\text{Fe}^{2+}$  also shows some residual absorption at this wavelength, for this reason the difference of molar absorptivities of these two ions is necessary;  $\Delta\epsilon = 2201 \text{ M}^{-1}\text{cm}^{-1}$ . As a result of irradiation,  $\text{Fe}^{3+}$  accumulates linearly with dose for the dose range up to 400 Gy, so that the slope of the plot  $\text{OD}_{304}$  vs. time,  $d[\text{OD}_{304}]/dt$ , is proportional to the dose rate,  $dD/dt$ , where D is the dose.

One hundred  $\mu\text{L}$  of 1 mM  $\text{FeSO}_4$  in 0.4M  $\text{H}_2\text{SO}_4$  was placed in 2 mL ampoules and irradiated during different radiation times (0, 10, 20, 30, 40, 50, and 60 s). Each of these samples was analyzed spectrophotometrically between 450 nm to 250 nm for accumulation of  $\text{Fe}^{3+}$ . A linear regression of absorbance against time was plotted and the slope was determined. With the slope (rate of change of absorbance with time), rate of accumulation of  $\text{Fe}^{3+}$  was determined using the Beer-Lambert Law. The rate of accumulation of  $\text{Fe}^{3+}$  was obtained by relating to the dose rate and the radiation chemical yield of  $\text{Fe}^{3+}$  ( $1.5 \times 10^{-6}$  x mol/J), which is well known.<sup>121</sup>

#### X-Irradiation Procedure and Illumination Procedures

In a typical experiment, 100  $\mu\text{L}$  of the DNA solution of a given concentration in 10 mM phosphate buffer, pH 6.9, with or without additives depending on the experiment was placed in a 2mL flat bottom Wheaton ampoule. The samples were irradiated at room temperature from the bottom with X-ray from a Philips tube with a tungsten anode. The tube was run at a voltage of 55 kV and 20 mA that produced a dose of 9.77Gy/s (measured by Fricke dosimetry). DNA aqueous solutions were irradiated at doses from 100 Gy to 24 kGy.

For UV illumination 600  $\mu\text{L}$  of the DNA solution of a given concentration in 10 mM phosphate buffer, pH 6.9, with additives were placed in a 2 mL glass vial. Samples were then transferred into a beaker containing water and illuminated at room temperature from the side with a high Hg(Xe) lamp at a voltage 20 V and 6 A while stirring continuously with a flea bar. DNA aqueous solutions were irradiated at times from 60 s to 1800 s.

## DNA Hydrolysis

After irradiation or illumination the DNA solutions were lyophilized for about 30 min. Immediately after that, 200  $\mu\text{L}$  of 88% formic acid was added. The samples were deaerated by two freeze-pump-thaw cycles to avoid further oxidation of guanine and 8oxoG. Samples were then sealed and hydrolyzed for 90 min at 150°C. During heating DNA samples with formic acid, complete DNA hydrolysis occurs with the nearly quantitative release of all nucleobases, both modified during irradiation and unaltered. Then after cooling, the ampoules were open and lyophilized for 1h. The samples were reconstituted by adding 100  $\mu\text{L}$  of 100 mM NaOH and allowed to stand for 15 min. Nine hundred  $\mu\text{L}$  of 40mM ammonium acetate was then added. Ampoules were resealed and left overnight at room temperature for equilibration.

## DNA Concentration Dependence Experiments

These experiments were conducted to examine the effect of DNA concentration on the production of 8oxoG in irradiated DNA. A 10 mM stock solution salmon testes DNA in 10 mM phosphate buffer, pH 6.9, was diluted using the same buffer to make 5 mM, 2 mM, and 1 mM DNA solutions. These samples were then treated as described above.

## The Effect of Different DNA Hole Injectors

- A.  $\bullet\text{OH}$  Radicals. Formation of 8oxoG as a result of DNA oxidation by the  $\bullet\text{OH}$  radicals was studied by X-irradiating different concentrations of salmon testes DNA in 10 mM phosphate buffer, pH 6.9, without any additives.
- B.  $\text{Br}_2\bullet$  Radicals. Formation of 8oxoG as a result of DNA oxidation by the  $\text{Br}_2\bullet$  radicals was studied by X-irradiating different concentrations of salmon testes DNA and other

DNA types in 10 mM phosphate buffer, pH 6.9 in the presence of 100 mM sodium bromide.

C.  $SO_4^{\bullet-}$  Radicals. Seven hundred twenty  $\mu\text{L}$  of 10 mM salmon testes DNA in phosphate buffer was placed in a transparent sample vial. Eighty  $\mu\text{L}$  of 100 mM  $K_2S_2O_8$  was added to the DNA solution immediately before illumination. The vial was immersed in a beaker with water at room temperature to avoid heating the sample during illumination. The control sample (no illumination) was kept at room temperature during the longest time of illumination. The samples were photolyzed with the Xe(Hg) lamp under constant stirring for up to 15 min. After illumination, 200  $\mu\text{L}$  of samples were placed in an ampoule using a pasture pipette and 20  $\mu\text{L}$  of saturated protamine was added to precipitate DNA. The sample was then vortexed gently and centrifuged. The precipitate was then collected and washed with 1 mL deionized water and the supernatant discarded. Washing the samples was necessary to eliminate  $K_2S_2O_8$  from the solution to avoid further oxidation of DNA by  $K_2S_2O_8$  during hydrolysis. After that, the samples were treated as previously described.

D.  $CO_3^{\bullet-}$  Radicals i) A solution of carbonatopentamminecobalt (III) perchlorate was prepared in 10 mM phosphate buffer with an optical density (OD) at maximum of 0.3-0.5. The concentration of the complex was calculated from its OD ( $\epsilon = 70 \text{ M}^{-1}\text{cm}^{-1}$ ). The complex was prepared fresh right before every experiment because of the unstable nature of the compound. A master solution was prepared with 5 mM DNA and 2 mM cobalt complex in a 10 mM phosphate buffer, pH 6.9. The samples were then illuminated in a tube immersed in a beaker with water with constant stirring. The current was kept at 6 A.



After illumination for an appropriate amount of time, the samples were kept on ice. Two hundred  $\mu\text{L}$  of each sample was placed into an ampoule and treated as previously described.

ii) Ninety  $\mu\text{L}$  of salmon testes DNA dissolved in 340 mM  $\text{NaHCO}_3$  (10 $\mu\text{L}$  100 mM  $\text{K}_2\text{S}_2\text{O}_8$ ) solution was placed in 2mL flat bottom ampoule. Ten  $\mu\text{L}$  100 mM  $\text{K}_2\text{S}_2\text{O}_8$  was added to the ampoule immediate prior to irradiation. The samples were X-irradiated at required doses. DNA was precipitated using 20  $\mu\text{L}$  saturated protamine. The samples were gently vortexed and centrifuged. The precipitate was collected and washed with 1 mL of distilled water and the supernatant was discarded. After that, the samples were processed as previously described.

### Oxygen Dependence Experiments

Oxygen dependence experiments were performed with 10 mM salmon testes DNA in the presence of 100 mM sodium bromide or without any additives. The samples designated as ‘without oxygen’ were deaerated prior to X-irradiation by two freeze-pump-thaw cycles and then sealed under pumping before X-irradiation and then processed as previously described.

### The Effect of Different DNA Content

Both native and synthetic highly polymerized DNA with different CG content were employed to study the effect of the CG content and of the base sequence on the yields of 8oxoG. In these experiments, 1 mM, 2.5 mM or 0.72 mM DNA were used in the presence of 100 mM NaBr. The following DNA types were tested: salmon testes DNA, micrococcal DNA, poly(CG-GC), and poly(CC-GG).

## HPLC Analysis

HPLC Analysis of Authentic 8oxoG as a Reference. The dilutions of authentic 8oxoG described in section 2 of the current chapter were analyzed by HPLC to determine the linearity of the HPLC response of 8oxoG and to determine the saturation limit of 8oxoG. This information helped to compare the concentration of 8oxoG in our samples to the saturated 8oxoG.

HPLC Conditions for the Analysis of 8oxoG. Typically, 200  $\mu\text{L}$  of samples were transferred into HPLC vials and analyzed by the reverse phase HPLC on a Gemini 250 $\times$ 4.6mm 5 $\mu$  C18 analytical column (Phenomenex) operated at 30 $^{\circ}\text{C}$  and equilibrated with 40 mM ammonium acetate pH 6.9. Typically, the injection volumes were 100  $\mu\text{L}$ . A linear 80% acetonitrile gradient (11% over 10 min at a flow rate of 1mL/min) was applied to elute the products. Identification of products was based on the comparison of retention times of authentic reference compounds and of their UV-Vis spectra.

Calculations of Concentrations of 8oxoG. The extinction coefficients of all four DNA bases have been previously determined spectrophotometrically by our research group (Table 3).

**Table 3.** The experimentally determined extinction coefficients of DNA bases at 254 nm and 8oxoG and G at 305 nm in 40 mM ammonium acetate solution, pH 6.9

Bases	Extinction Coefficient ( $M^{-1}cm^{-1}$ )	Extinction Coefficient ( $M^{-1}cm^{-1}$ )
	at 305 nm	at 254 nm
8oxoG	3458	-
Guanine	321.6	9280
Adenine	-	11990
Cytosine	-	5070
Thymine	-	6690

The concentration of 8oxoG was calculated from the chromatographic peak areas of 8oxoG and adenine (Ade) using the following equation:

$$[8oxoG] = \frac{A_{305}(8oxoG)}{A_{254}(Ade)} \times \frac{\epsilon_{254}(Ade)}{\epsilon_{305}(8oxoG)} \times [Ade] \quad (14)$$

where  $A(Ade)$  is the area of the adenine chromatographic peak at 254 nm,  $A(8oxoG)$  is the area of the 8oxoG chromatographic peak at 305 nm,  $\epsilon_{254}(Ade)$  is the extinction coefficient of adenine at 254 nm, and  $\epsilon_{305}(8oxoG)$  is the extinction coefficient of 8oxoG at 305 nm, and  $[Ade]$  is the concentration of adenine calculated based on the content of a given type of DNA and on the concentration of DNA in the sample.

The choice of adenine as an internal standard was made by using the assumption that, unlike guanine that is oxidized in course of the reaction, the concentration of adenine practically does not change during DNA oxidation. The reproducibility of the peak area of adenine for a given concentration of DNA and its independence of the irradiation/illumination dose has been experimentally confirmed in the present study. For poly (CG-GC) and poly (GG-CC), because of the absence of adenine in this type of DNA, concentration of 8oxoG was calculated using the following equation:

$$[8oxoG] = \frac{A_{305}(8oxoG)}{A_{254}(G)} \times \frac{\epsilon_{254}(G)}{\epsilon_{305}(8oxoG)} \times [G] \quad (15)$$

where  $A(G)$  is the area of the guanine chromatographic peak at 254 nm, and  $\epsilon_{254}(G)$  is the extinction coefficient of guanine at 254 nm and  $[G] = 0.5$  mM because the content of G in this type of DNA is 50% and 1 mM DNA was used.

## CHAPTER 4

### RESULTS AND DISCUSSION

#### Optimizing Conditions for Quantitative Detection of 8oxoG

##### The rationale for using 305 nm as the wavelength for HPLC detection of guanine and 8oxoG

Because of the structural similarity, HPLC retention times of guanine and 8oxoG are very close, so resolving these two peaks can be challenging. So, it is important to optimize HPLC conditions for the maximum resolution of guanine and 8oxoG for quantitative detection of the latter. It is also important to keep in mind that the amount of 8oxoG released from oxidatively damaged DNA is much lower than the amount of non-modified guanine, so it is reasonable to detect both peaks at a wavelength at which the ratio of extinction coefficients of 8oxoG and G is the largest. It can be seen from Figure 14 that though UV-Vis spectra of G and 8oxoG are quite similar, the second peak maximum of 8oxoG is significantly shifted towards longer wavelength as compared to that of guanine. Analysis of UV-Vis spectra of both compounds showed that at 305 nm  $\epsilon(\text{G})/\epsilon(\text{8oxoG})$  is the largest so 305 nm was chosen as a working wavelength for HPLC detection of 8oxoG and G.

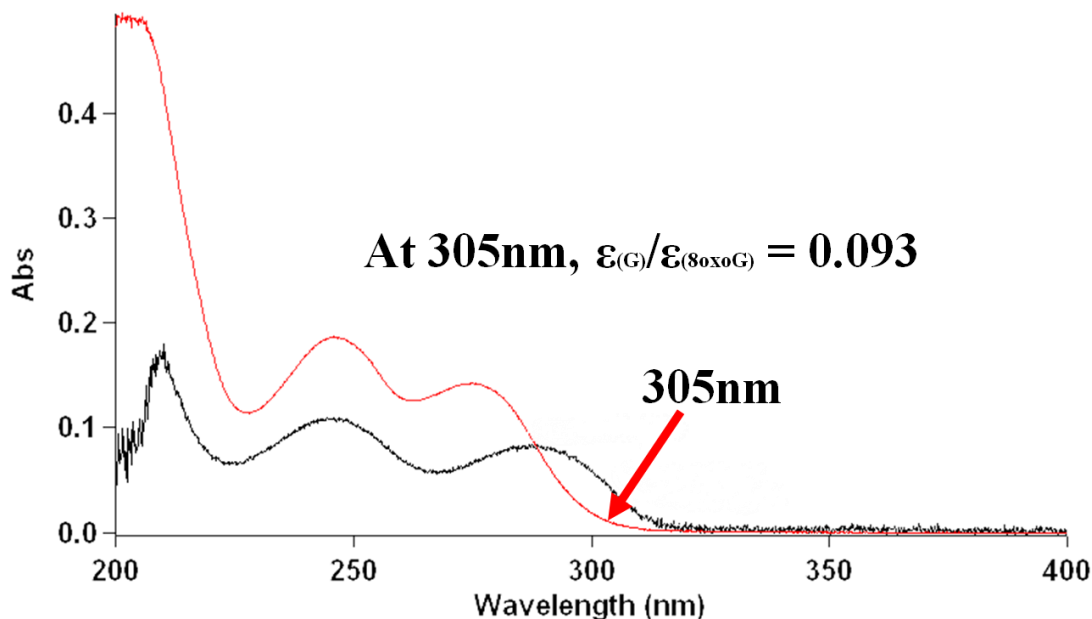


**Figure 14.** The superimposition of the UV-Vis spectra of guanine (red trace) and 8oxoG (black)

Determining the extinction coefficient of 8oxoG at 305nm

The extinction coefficient of 8oxoG at 305nm was determined as is described in Chapter 3. UV-Vis spectra of a series of dilutions of saturated solution of 8oxoG were obtained and absorbencies at 305 nm were plotted as a function of absorbencies at 285 nm (Figure 15). The extinction coefficient of 8oxoG at 305 nm was calculated to be  $3.46 \times 10^3 \text{ M}^{-1}\text{cm}^{-1}$  (see Appendix A) from the linear regression equation as shown below.

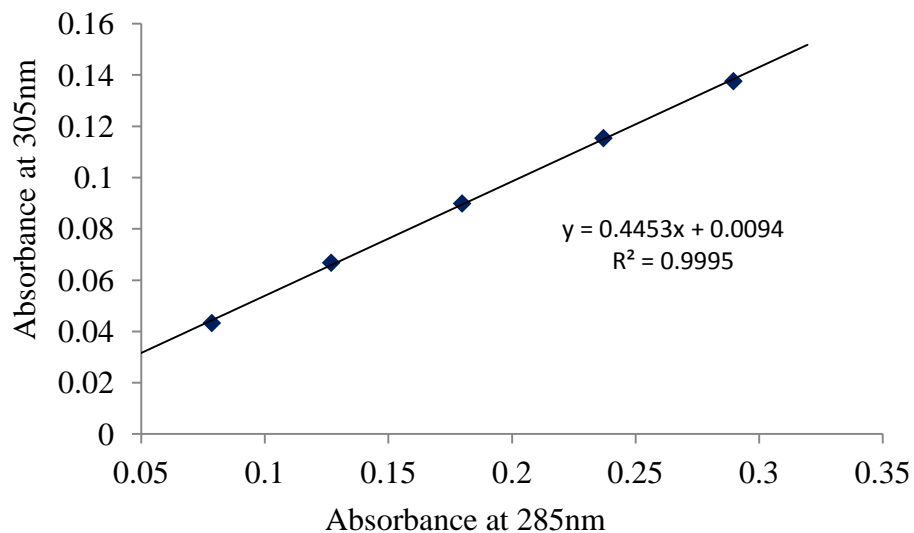


**Figure 15.** The linear regression of the absorbance of authentic 8oxoG solution in 40 mM ammonium acetate, pH 6.9 at 305 nm vs. absorbance at 285 nm

#### Linearity of 8oxoG

A series of dilutions of saturated solution of authentic 8oxoG was analyzed by HPLC to determine the linearity of the HPLC response of 8oxoG and to determine the saturation limit of 8oxoG (Figure 16).

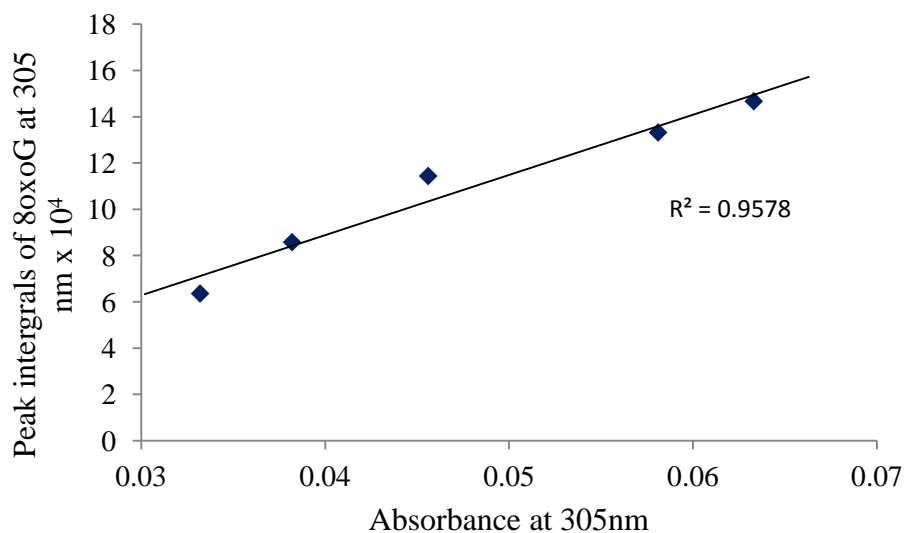


**Figure 16:** The calibration curve of the HPLC peak integrals of reference 8oxoG vs concentration of 8oxoG expressed as fold dilutions of saturated solution of 8oxoG

### Fricke Dosimetry

This technique is helpful to convert irradiation times in seconds to radiation dose in Gray (Gy). This employs the principle of the chemical method of conversion of  $\text{Fe}^{2+}$  into  $\text{Fe}^{3+}$ .  $\text{Fe}^{2+}$  was irradiated during various irradiation times. Samples were then analyzed by UV spectrophotometer between 450 nm to 250 nm for accumulation of  $\text{Fe}^{3+}$ . A linear regression of the absorbance at 304 nm which typically is the maximum for  $\text{Fe}^{3+}$  was plotted against irradiation time and subsequently slope was obtained (Figure 17). The extinction coefficient of  $\text{Fe}^{3+}$  was obtained as the difference between that of  $\text{Fe}^{3+}$  and  $\text{Fe}^{2+}$  ( $\Delta\epsilon = 2201 \text{ M}^{-1}\text{cm}^{-1}$ ). This was because  $\text{Fe}^{2+}$  has the tendency of absorbing at the maximum wavelength of 304 nm. The dose rate was calculated as 9.77 Gy/s using the Beer-Lambert law a more detailed description given in Appendix B).



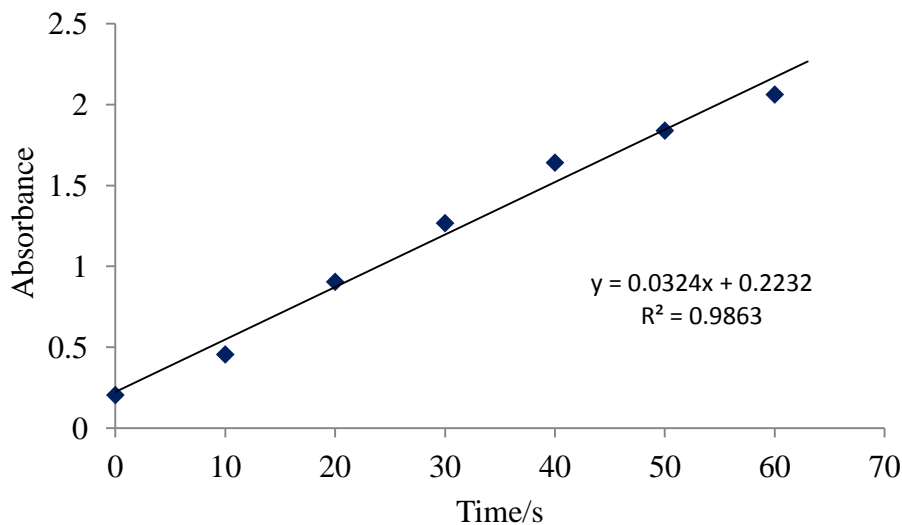


**Figure 17.** Fricke dosimetry dose-response curve. See the text and Appendix B for details

#### Optimizing of HPLC Conditions for Detection of 8oxoG

We found out experimentally that HPLC conditions described in Chapter 3 (a linear gradient of acetonitrile from 0 to 8.8 % during 10 min at a flow rate of 1 mL/min) provide a good resolution of peaks of 8oxoG and G (see Figure 19 that shows a representative chromatogram of a mixture of authentic 8oxoG and G) which is essential for the quantitative analysis of 8oxoG and G. In a typical chromatogram of the mixture of G and 8oxoG, the retention times were ~ 10.2 and ~10.8 min, respectively. As can be seen in Figure 18 the peaks for 8oxoG and G are completely resolved under these conditions, so that both compounds can be easily quantified by HPLC peak integration.

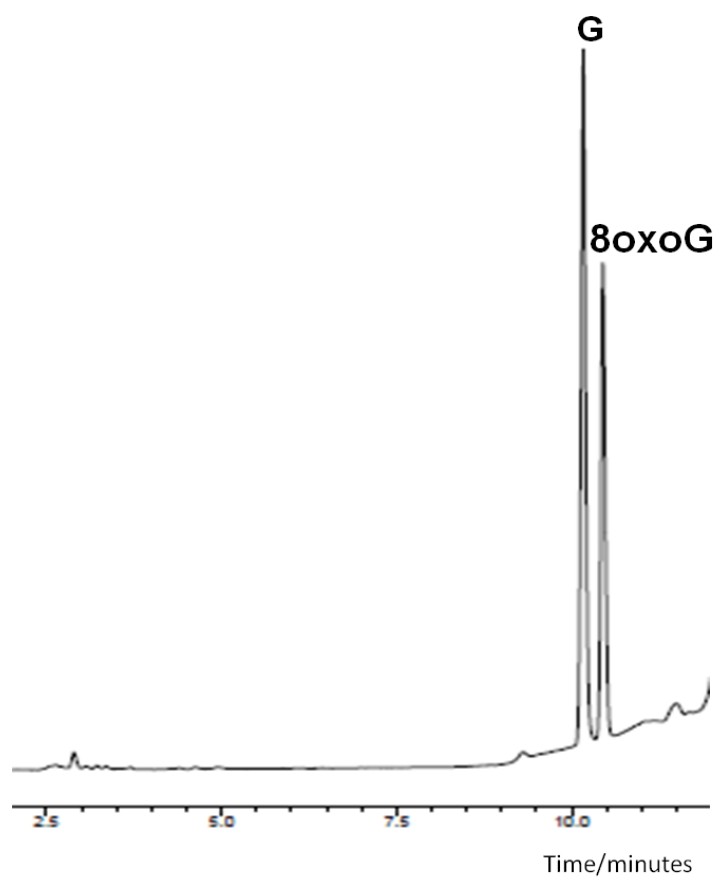


**Figure 18:** A representative chromatogram of a mixture of authentic 8oxoG and G.

HPLC conditions used: Reverse phase HPLC C18 column; equilibrated with 40mM ammonium acetate; linear gradient of acetonitrile from 0 to 8.8 % during 10 min at a flow rate of 1 mL/min.

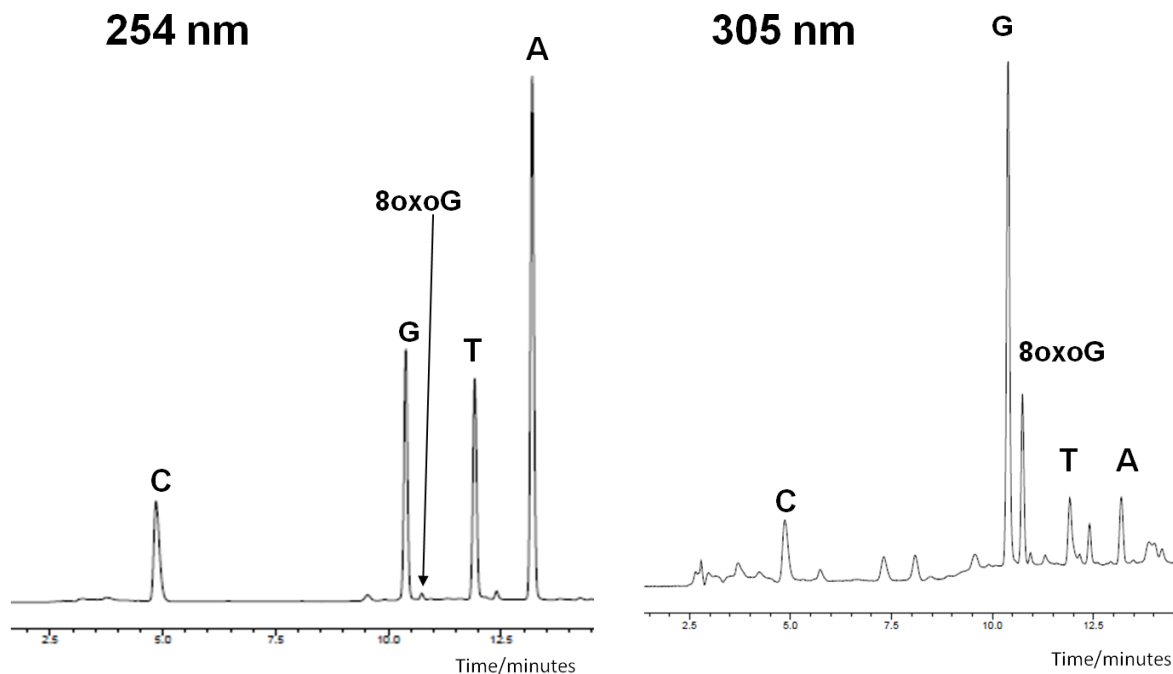


**Figure 19:** Representative chromatogram shown at two different wavelengths (and on different scales) for 2 mM salmon testes DNA X-irradiated at 5.3 kGy in 10 mM phosphate buffer, pH 6.9 in the presence of 100 mM NaBr and then hydrolyzed in hot formic acid as described in Chapter 3. HPLC conditions are the same as in Figure 18.

Figure 19 shows a representative chromatogram of the supernatant prepared from native DNA hydrolyzed in formic acid. The left panel shows all four DNA bases detected at 254 nm. In this range of wavelengths, the absorptions of DNA bases and of 8oxoG are close to their maxima, so this chromatogram shows a realistic ratio of DNA bases and 8oxoG when their respective extinction coefficients are taken into account, see Table 2. As shown below in Figure 20 the yield 8oxoG in irradiated DNA is in the range of 2-2.5% of the yield of G. The right panel shows the same chromatogram but at 305 nm, at which the peak for 8oxoG is emphasized.

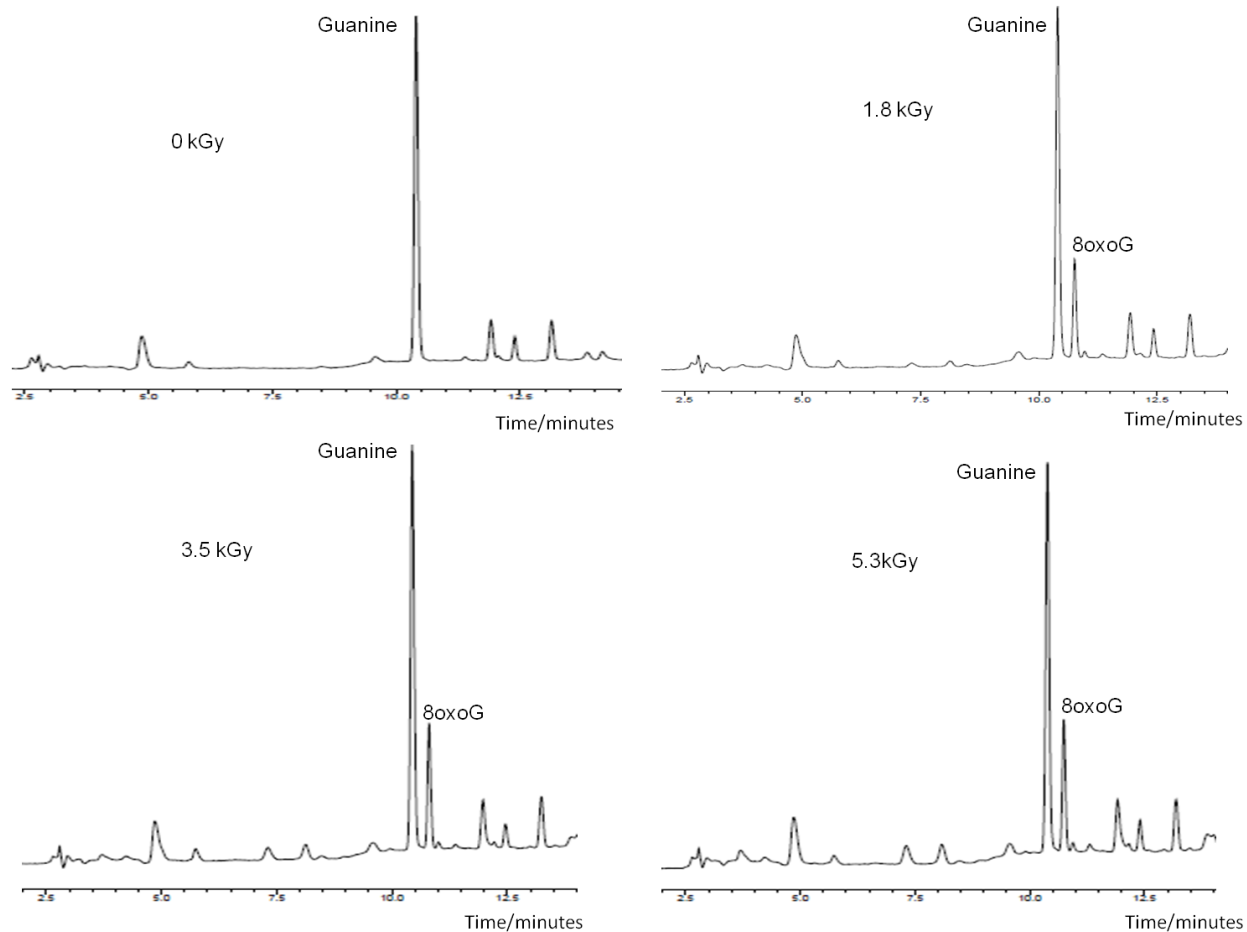


**Figure 20:** Accumulation of 8oxoG in an aqueous solution of salmon testes DNA irradiated in the presence of 1 M NaBr at various radiation times. Conditions: 2 mM (in bases) solution of DNA in 10 mM phosphate buffer, pH 6.9 was X- irradiated at indicated doses and then hydrolyzed in hot formic acid as described in Chapter 3.

Representative chromatograms in Figure 20 for 2mM salmon testes DNA at different doses illustrate the accumulation of 8oxoG formed in DNA with radiation dose increase from 0 (no irradiation) to 5.3 kGy. Importantly, no 8oxoG formation can be detected for non-irradiated DNA, while the yield of 8oxoG is increased with dose.

### The Effect of DNA Concentration on Production of 8oxoG

This series of experiments on DNA concentration dependence has been designed to answer the question whether the steady state yield of 8oxoG depends on DNA concentration. Ten mM stock solution of salmon testes DNA was diluted with 10 mM phosphate buffer, pH 6.9 to 1, 2, and 5 mM (in bases). The samples were X-irradiated in the presence of 0.1 M NaBr. The ratio of [8oxoG]/[G] was calculated using the Equation 14 from Chapter 3. The ratio of [A]/[G] in salmon testes DNA is equal to the AT:CG ratio in the DNA sample: [A]/[G] = 1.38.

The ratio of [8oxoG] to [G] was calculated for all the four concentrations of DNA and plotted as a function of dose (Figure 21). Error bars are not shown on these plots but are shown in Figure 22 below. All dose dependence curves show a sigmoid shape, with a pronounced saturation region after ~ 2 kGy. The steady state is reached quickly and corresponds to about one 8oxoG per 60 G (one 8oxoG per ~120 bp). Such a low steady state cannot be explained by simple competition between 8oxoG and G for the incoming  $\text{Br}_2^{\bullet-}$ . A mechanism suggesting further hole transfer from  $\text{G}^{\bullet+}$  to 8oxoG has to be invoked.

To determine radiation chemical yields ( $\Gamma$ ) of 8oxoG, the ratios of [8oxoG]/[G] were plotted as a function of dose for the initial period of 8oxoG accumulation for different concentrations of DNA (shown in Appendix 3). The slopes of the linear regression trend lines were obtained to be  $1.77 \times 10^{-5}$ ,  $2.66 \times 10^{-5}$ ,  $2.22 \times 10^{-5}$ , and  $1.42 \times 10^{-5}$  kg/J for 1, 2, 5, and 10 mM DNA, respectively, and the radiation chemical yields of 8oxoG were calculated using Equation 16:

$$\Gamma = \text{slope} \times [G] \quad (16)$$

where  $\rho = 1 \text{ kg/L}$ , and  $[G]$  in 1 mM, 2 mM, 5 mM, and 10 mM solutions are 0.21mM, 0.42 mM, 1.05 mM, and 2.1 mM, respectively. Radiation chemical yields of 8oxoG are summarized in Table 4.

**Table 4.** The radiation chemical yields of 8oxoG for different DNA concentrations

Salmon Testes DNA Concentration (mM)	Radiation Chemical Yield of 8oxoG (nmol/J)
1	3.7
2	11.2
5	23.3
10	29.8

Since the initial rate of accumulation of 8oxoG expressed as the ratio  $[8oxoG]/[G]$  is essentially the same for all four DNA concentrations tested, it means that the initial rate of accumulation of 8oxoG increases with DNA concentration. This increase is reflected as the increase of the radiation chemical yields of 8oxoG formation (Table 4) with DNA concentration. However, initial rates of 8oxoG accumulation with dose and hence radiation chemical yields of 8oxoG are supposed to be independent of the concentration of DNA in the solution because DNA is in a large excess to the dibromide radical anions and the concentration of  $Br_2^{\bullet-}$  is maintained at a low steady state level, which can be easily shown by comparison of reaction rate constants of formation of  $Br_2^{\bullet-}$  (see reactions 5-7 in Chapter 2). The increase in radiation chemical yields of 8oxoG with DNA concentration shown in Table 4 can be explained by a non-homogeneous kinetics of dibromide radical anion with guanines in DNA. Indeed, the assumption of homogeneously distributed guanines in the solution is an oversimplification because actually

guanines are tethered to polymeric DNA molecules rather than are freely distributed in the solution.

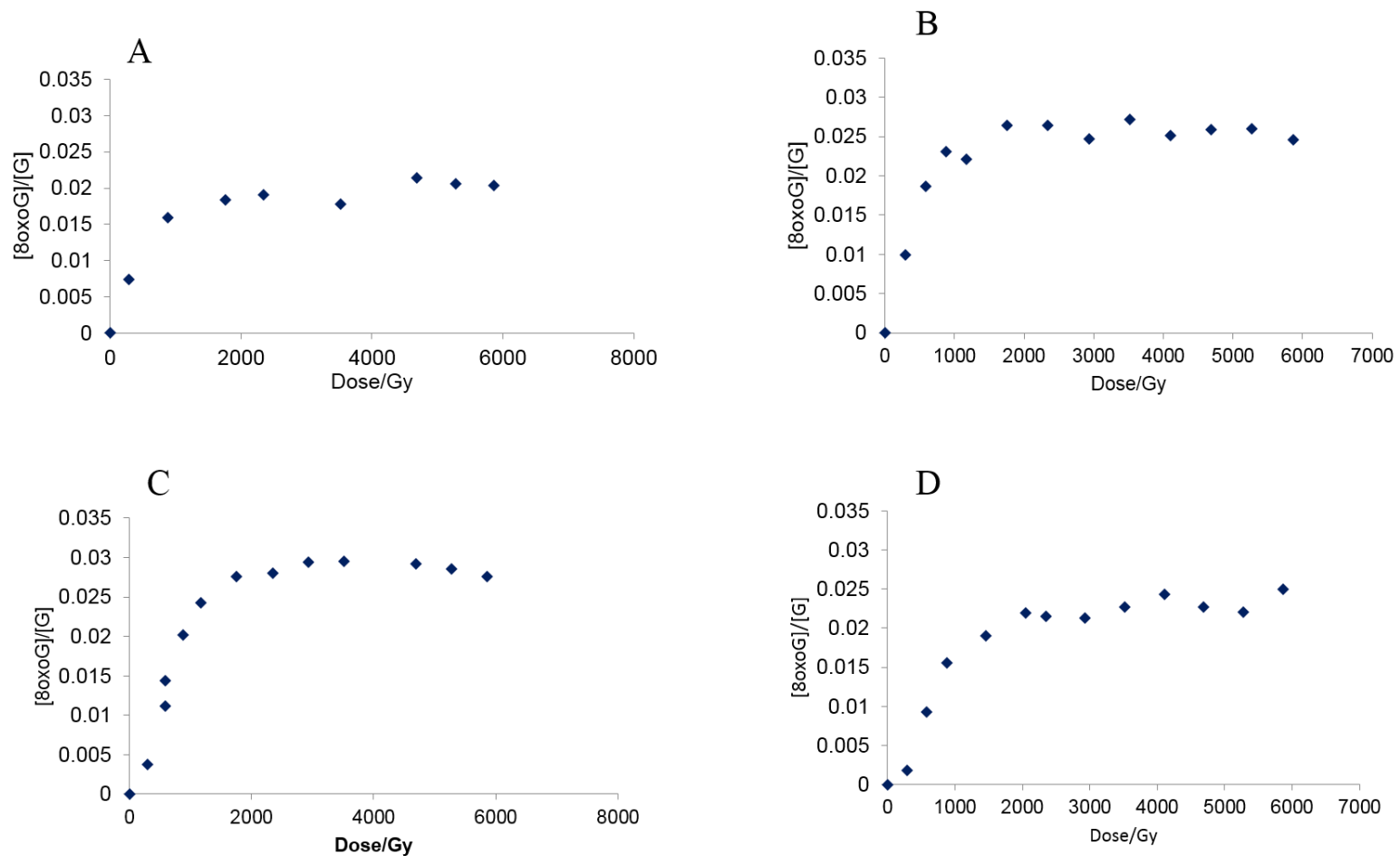


**Figure 21.** Yields of 8xoG as a function of dose for the following concentrations of salmon testes DNA (in nucleotides): **A.** 1 mM; **B.** 2 mM; **C.** 5 mM; **D.** 10mM. DNA solutions were irradiated in the presence of 100 mM NaBr and then treated as described in Chapter 3.



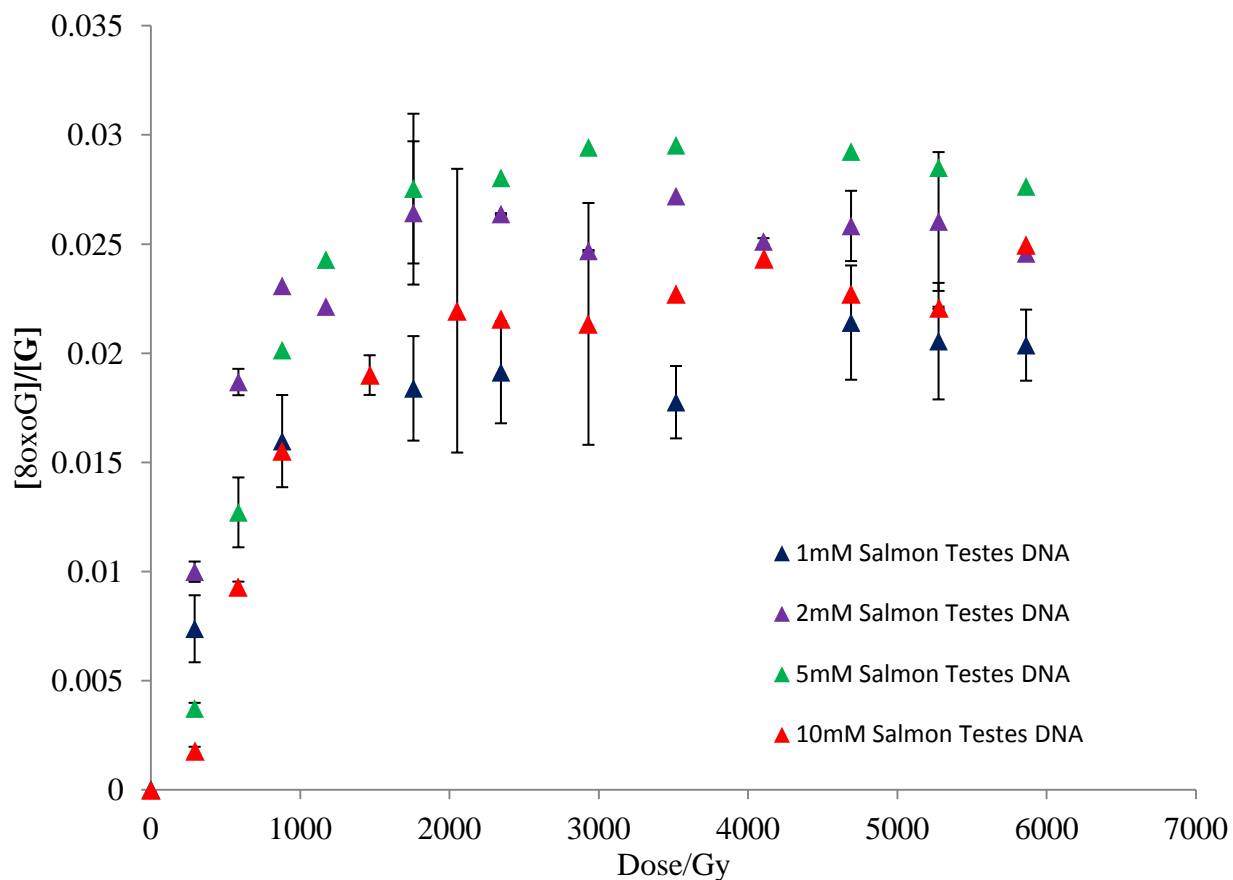


**Figure 22:** Accumulation of 8oxoG in X-irradiated salmon testes DNA for various concentrations of DNA. DNA solutions were irradiated in the presence of 100 mM NaBr and then treated as described in Chapter 3.

Figure 22 shows the dose dependence curves for 8oxoG production for all four DNA concentration tested. Most of the data in Figure 22 have been calculated as the averages from two or three experiments, with the respective error bars. Some error bars are too small and hence are not visible on the plot. The steady state yield of 8oxoG is in a rather narrow range of ~ 2.0-2.8% of the initial amount of G in DNA for all four DNA concentration tested. One can see from Figure 22 that the steady state yields of 8oxoG decrease in the order 5 mM DNA > 2 mM DNA

> 10 mM DNA > 1 mM DNA, but these differences are not statistically significant. So it appears that the steady state yields of 8oxoG expressed as  $[8oxoG]/[G]$  are rather insensitive to DNA concentration in the range of DNA concentrations tested. The important corollary from these data is that any DNA concentration in this range can be used for the further experiments, which is important when very expensive synthetic polymerized DNA is used. In this case, it is desirable to use the lowest possible concentration of DNA. It has to be noted, however, that results are less reproducible with 1 mM DNA than with higher concentrations of DNA.

### The Effect of the Nature of Oxidant on the Production of 8oxoG

In this section, 5 mM or 10 mM solutions of salmon testes DNA were used. Oxidants were produced by either X-irradiation ( $\bullet OH$ ,  $Br_2^{\bullet -}$ ,  $CO_3^{\bullet -}$ ,  $SeO_3^{\bullet -}$ , and  $(SCN)_2^{\bullet -}$ ) or by UV-photolysis ( $SO_4^{\bullet -}$ ,  $CO_3^{\bullet -}$ ). Although it is difficult to compare initial rates of 8oxoG accumulation for different methods of hole generation, the steady state yields of 8oxoG can be compared for different oxidants and different methods of hole injection under the assumption of the model described in Chapter 2 that once a hole is injected into a DNA array, its further fate only depends on the DNA sequence and structure.

#### Dibromide Radical Anion, $Br_2^{\bullet -}$

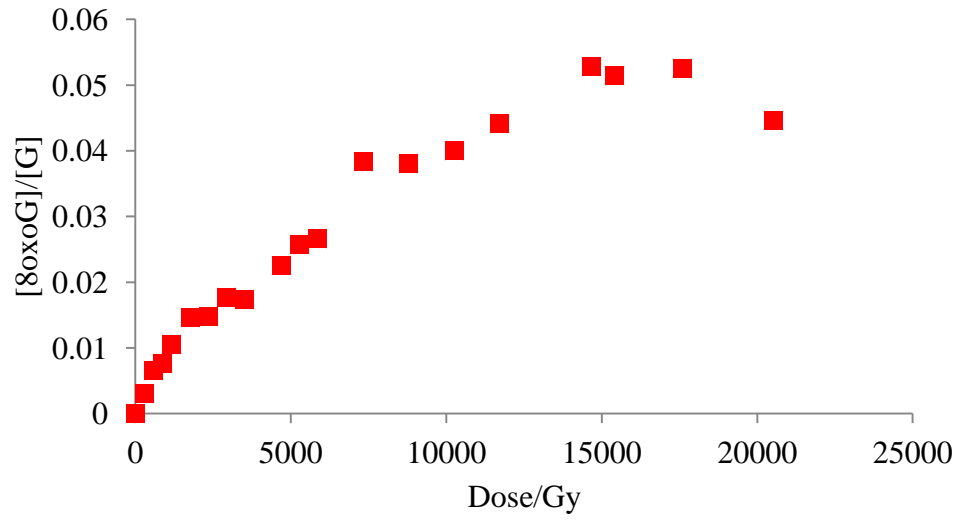
The plots of 8oxoG accumulation for DNA oxidized by  $Br_2^{\bullet -}$  are shown in the previous section in Figure 23. The approximate average yield of 8oxoG for 5 mM and 10 mM DNA is ~ 2.5% of total guanine.

## Hydroxyl Radical •OH

Hydroxyl radical is the strongest oxidant in neutral solutions under consideration; similar to the sulfate radical anion, it oxidizes DNA bases indiscriminately.

Hydroxyl radicals can be efficiently generated from water with the radiation chemical yield of  $0.265 \mu\text{mol/J}^{21}$  by radiolysis of aqueous solutions. Ten mM (in nucleotides) solutions of salmon testes DNA in 10 mM phosphate buffer, pH 6.9 were X-irradiated at different doses. It can be seen from Figure 24A and B that 8oxoG accumulation plateaus off at much higher radiation doses for •OH as compared to  $\text{Br}_2^{\bullet-}$ . On the contrary, the region of initial accumulation of 8oxoG (Figure 23C) indicates a slower accumulation by •OH as compared with  $\text{Br}_2^{\bullet-}$ . This result can be explained because  $\text{Br}_2^{\bullet-}$  only reacts by outer sphere electron transfer (Figure 1, bottom reaction of guanine) forming mobile holes  $\text{G}^{\bullet+}$  that can either migrate or convert into 8oxoG. Thus in this case [8oxoG] reaches a steady state fast. The precursors for 8oxoG are generated at a slower rate in the case of •OH, that is consistent with that •OH predominately reacts with DNA by double bond addition to nucleobases to form an  $\text{G(OH)}^{\bullet}$  radical adduct (Figure 1, top reaction of guanine), that can be regarded to as 'fixed holes' because they cannot directly participate in electron transfer. Thus in the case of reaction with •OH, initial accumulation of 8oxoG occurs slower than in the reaction with  $\text{Br}_2^{\bullet-}$  because the process of outer sphere electron transfer occurs significantly faster than addition to double bonds. However, the steady state of 8oxoG is higher (if reached at all) in the case of reaction with •OH, indicating the lack of hole mobility, so that all  $\text{G(OH)}^{\bullet}$  adducts convert into 8oxoG via deprotonation and the second one-electron oxidation (most likely by reaction with molecular oxygen).

**A**



**B**

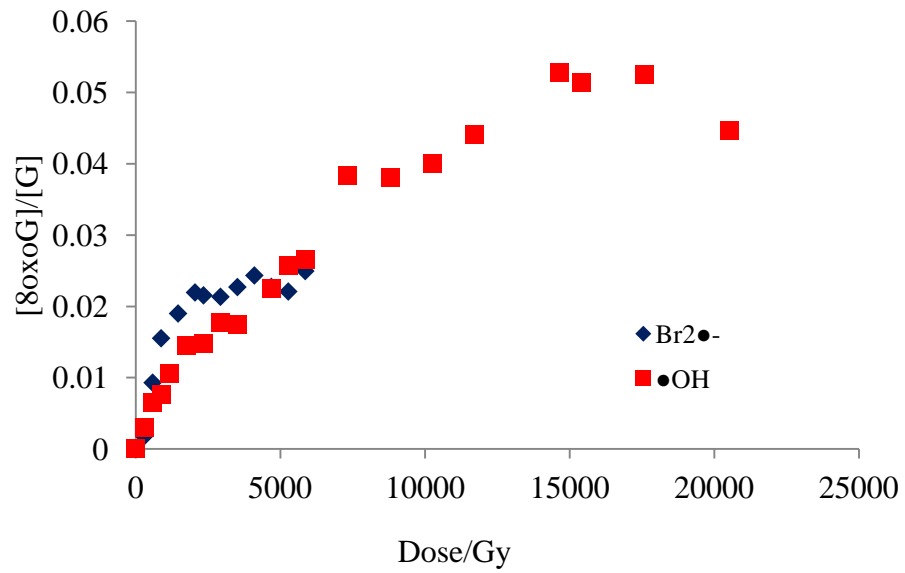
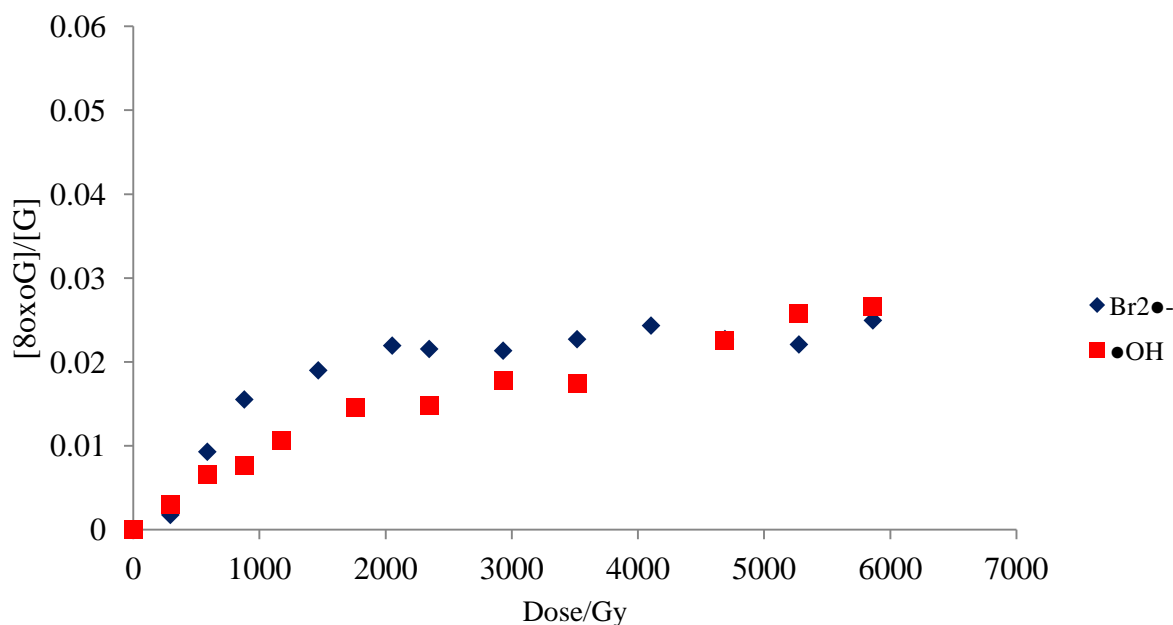


Figure 23 (continued on the next page)

C



**Figure 23.** Comparison of accumulation of 8oxoG produced as a result of DNA oxidation by hydroxyl radicals ( $\bullet\text{OH}$ ) and the dibromide radical anions ( $\text{Br}_2\bullet^-$ ). **A.** A total plot for  $\bullet\text{OH}$ ; **B.** Total plots for  $\text{Br}_2\bullet^-$  and  $\bullet\text{OH}$ ; **C.** Initial regions for  $\text{Br}_2\bullet^-$  and  $\bullet\text{OH}$ .

#### Sulfate Radical Anion $\text{SO}_4\bullet^-$

$\text{SO}_4\bullet^-$  in neutral solution is the second most powerful oxidant under consideration (after hydroxyl radical); it oxidizes DNA bases indiscriminately. Although the exact mechanism of oxidation of DNA bases by  $\text{SO}_4\bullet^-$  is unknown, the mechanism of addition to double bonds with formation of a base- $\text{SO}_4$  adduct and a subsequent elimination of sulfate anion was suggested<sup>21</sup>.

The sulfate radical anions were generated according to a well-known procedure described in Chapter 3. Ten mM (in nucleotides) of salmon testes DNA in 10 mM phosphate buffer, pH 6.9 with 100 mM  $\text{Na}_2\text{S}_2\text{O}_8$  and illuminated with the Hg(Xe) lamp at different times. The plot for

8oxoG accumulation as a function of the illumination time is shown in Figure 24. Interestingly, the graph reproducibly shows two plateau regions: one with the yield of 8oxoG to be of ~ 2.6% of the total G and the second one with the yield of 8oxoG to be of ~ 1.8% of the total G. The reason for formation of two plateaus is unknown; it should be kept in mind, though, that persulfate is itself a strong oxidant, so that direct oxidation of 8oxoG by the parent  $S_2O_8^{2-}$  or by  $SO_4^{\bullet-}$  for longer reaction times cannot be excluded. In this case, the steady state concentration of 8oxoG will decrease due to the further oxidation of 8oxoG into its products. An important observation is that the steady state yield of 8oxoG produced by  $SO_4^{\bullet-}$  is similar to that produced by  $Br_2^{\bullet-}$ ; both are in the narrow range of 2-2.5%. This indicates that the mode of mobile hole injection plays no essential role in the steady state yield of 8oxoG. The initial rates of formation of 8oxoG are not comparable for  $Br_2^{\bullet-}$  and  $SO_4^{\bullet-}$  because of the difference in generation techniques.

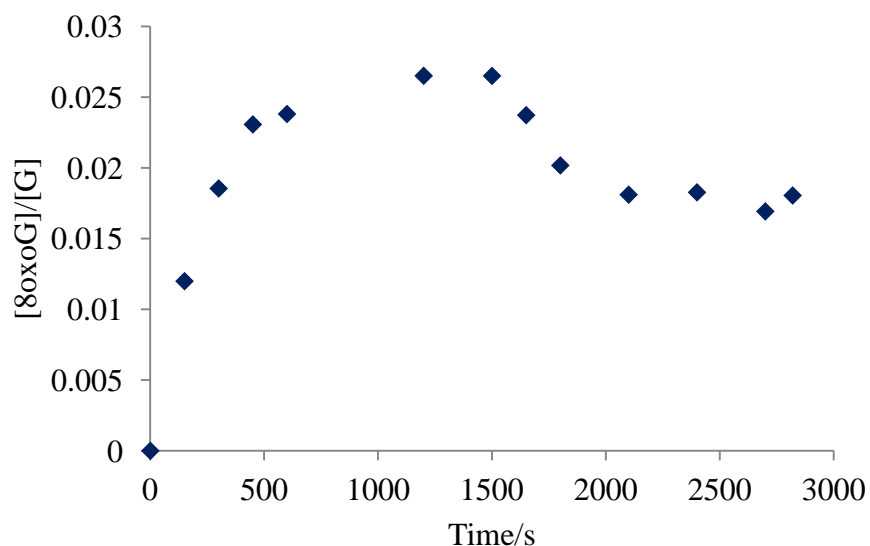


**Figure 24.** Accumulation of 8oxoG during DNA oxidation by  $SO_4^{\bullet-}$  produced by photolysis using the Hg(Xe) lamp of aqueous solution persulfate during indicated times. HPLC conditions were as previously indicated.

### Carbonate radical Anion, $\text{CO}_3^{\bullet-}$

Carbonate radical anion is a biologically relevant species with the reduction potential similar to that of  $\text{Br}_2^{\bullet-}$  (1.59 V vs 1.60V). It is known to react selectively with G.<sup>56</sup> However, the exact mechanism is unknown. Addition to the double bond with subsequent elimination was suggested, in particular, by Shafirovich et al.<sup>56</sup>

Two methods of generation of  $\text{CO}_3^{\bullet-}$  were used in the present work. In the Co(III) complex photodissociation method, 5 mM (in nucleotides) of salmon testes DNA in 10 mM phosphate buffer, pH 6.9 was illuminated in the presence of 2 mM carbonatopentamminecobalt (III) perchlorate. In the radiolysis of bicarbonate and persulfate mixture method, 10 mM salmon testes DNA dissolved in 300 mM  $\text{NaHCO}_3$  was X-irradiated in the presence of 10 mM  $\text{K}_2\text{S}_2\text{O}_8$ .

As Figure 25 demonstrates, both methods of production of carbonate radical anions resulted in a sigmoid shape of 8oxoG accumulation. However, the steady state level of 8oxoG is approximately 5-fold lower when carbonate radical anions were produced by photodecomposition of the cobalt complex (Figure 25A vs. Figure 25B). When using this complex, the rate of generation of carbonate radical anions is not steady and drops with time because of depletion of the Co complex, which likely explains the low steady state level of 8oxoG produced using this method. Thus, the plateau in Figure 25 A most likely does not indicate a 'true' steady state for 8oxoG.

However, the steady state yield of 8oxoG produced by carbonate radical anions generated by radiolysis of bicarbonate/persulfate is still more than 2-fold lower than when produced by dibromide or sulfate radical anions. The reason for this remains unclear, especially when taking into account very similar reduction potentials for  $\text{Br}_2^{\bullet-}$  and  $\text{CO}_3^{\bullet-}$  and analogous suggested mechanism of hole generation by  $\text{Br}_2^{\bullet-}$  and  $\text{SO}_4^{\bullet-}$ . Several problems, however, make it difficult

to compare  $\text{CO}_3^{\bullet-}$  with  $\text{Br}_2^{\bullet-}$  and other oxidants. The occurrence of side oxidation reactions of 8oxoG resulting in decrease of the steady state level of 8oxoG cannot be excluded. Also, the bicarbonate/persulfate method of generation of carbonate radical anions requires high concentrations of carbonate or bicarbonate, which shifts the pH and increases the ionic strength, which can affect the yield of 8oxoG.

A

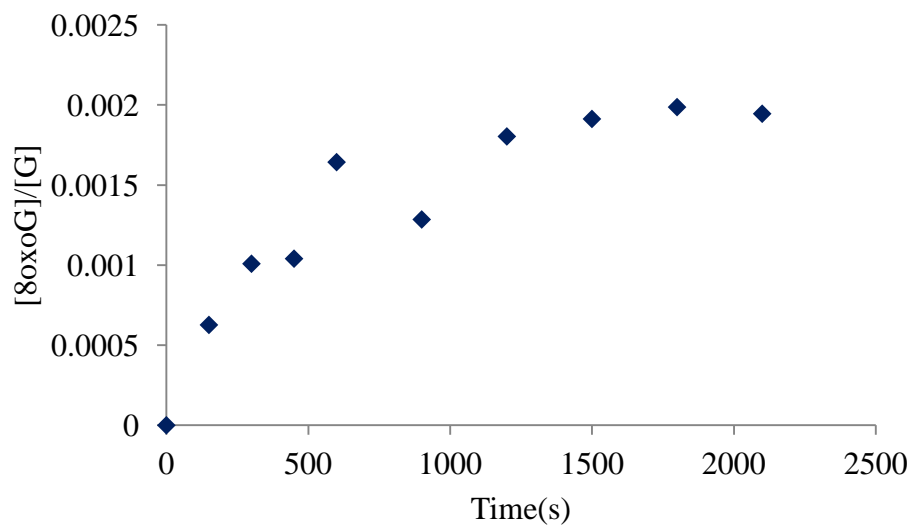
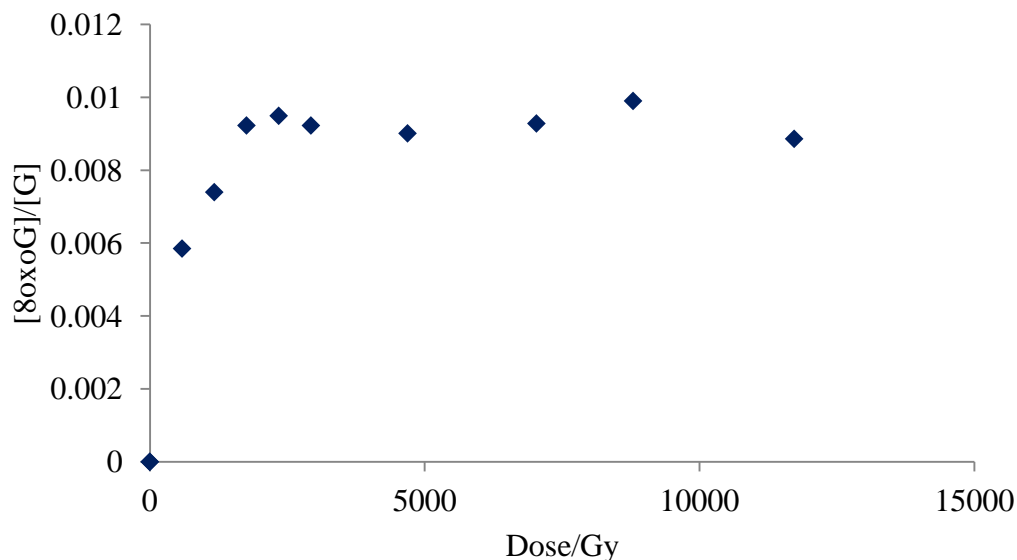


Figure 25 (continued on the next page)



**B**



**Figure 25:** Accumulation of 8oxoG produced by DNA oxidation by  $\text{CO}_3^{\bullet-}$  generated by:

**A.** Photolysis of 2mM carbonatopentamminecobalt (III) perchlorate; **B.** Radiolysis of aqueous solution of 300 mM  $\text{NaHCO}_3$  and 100 mM  $\text{Na}_2\text{S}_2\text{O}_8$ .

In general, the comparison of results of production of 8oxoG by hydroxyl radicals, dibromide radical anions, sulfate radical anions, and carbonate radical anions indicates that once a given oxidant generates a mobile hole in DNA ( $\text{G}^{\bullet+}$ ) (see the bottom reaction of guanine in Figure 1), steady state yield of 8oxoG is rather insensitive to the nature of the oxidant. Though both sulfate radical anions and carbonate radical anions are believed to react with DNA bases via the addition/elimination pathway (analogous to the reaction of hydroxyl radical with guanine, top reaction of guanine in Figure 1), the transient adducts are most likely very unstable and readily undergo elimination with the formation of  $\text{G}^{\bullet+}$ . Thus kinetically, reactions of guanine with sulfate radical anions and carbonate radical anions are very similar to the reaction of guanine with the dibromide radical anions and be described as electron transfer, though a true outer

sphere electron transfer may occur only in the case of dibromide radical anions. A different situation takes place for the reaction of guanine with hydroxyl radicals. Though hydroxyl radicals are known to be capable of direct electron transfer (bottom reaction of guanine in Figure 1), addition to double bonds (top reaction of guanine in Figure 1) remains a predominant mechanism. Contrary to sulfate and carbonate adducts,  $G(OH)^\bullet$  adduct is relatively stable because  $OH^-$  is not a good leaving group, so that the equilibrium  $G^{\bullet+} \leftrightarrow G(OH)^\bullet$  must be shifted towards formation of  $G(OH)^\bullet$ . Therefore, the reaction of hydroxyl radicals with guanine forms  $G(OH)^\bullet$  adducts as 'fixed' or immobile holes which cannot migrate by charge transfer. Thus, it is reasonable to assume that in this case 8oxoG is produced directly from the  $G(OH)^\bullet$  without formation of a mobile guanine radical cation as an intermediate.

It is also worth mentioning that dibromide radical anions and sulfate radical anions give very similar steady state yields of 8oxoG, though  $Br_2^{\bullet-}$  react selectively with guanines only while  $SO_4^{\bullet-}$  is indiscriminate towards all four DNA bases, as follows from their reduction potentials (see Table 2). This is explained by fast migration of a original hole formed at any DNA base and trapping by guanine as a hole sink, with formation of  $G^{\bullet+}$ .

#### Other Oxidants: $SeO_3^{\bullet-}$ and $(SCN)_2^{\bullet-}$

Theoretically, using  $SeO_3^{\bullet-}$  to generate 8oxoG looked promising because of their favorable oxidation potential ( $+1.77$  V),<sup>57</sup> see Table 1). However, results showed no accumulation of 8oxoG when  $SeO_3^{\bullet-}$  was used as a hole injector under the same experimental conditions described in Chapter 3, Section 3.3.1. Only the reaction of oxidation of Se (IV) has been tried (Reaction 17 in Chapter 2); while probably the reaction of reduction of Se (VI) is more efficient in production of  $SeO_3^{\bullet-}$ , which has not been attempted for technical reasons.

The use of  $(\text{SCN})_2^{\bullet-}$  showed no formation of 8oxoG. The absence of 8oxoG in this case can be attributed to a low reduction potential of  $(\text{SCN})_2^{\bullet-}$  (+1.33 V), which is too close the reduction potential of guanine (+1.29 V).

### The Effect of Oxygen on Production of 8oxoG

It is believed that formation of 8oxoG from its precursors is absolutely oxygen dependent.<sup>21</sup> The experiments on the effects of oxygen have been performed to elucidate whether the presence of oxygen affects accumulation of 8oxoG. These experiment were performed using  $\text{Br}_2^{\bullet-}$  or  $\bullet\text{OH}$  as hole injectors. 10 mM (in nucleotides) of salmon testes DNA in 10 mM phosphate buffer, pH 6.9 with (for  $\text{Br}_2^{\bullet-}$ ) or without (for  $\bullet\text{OH}$  radicals) 1M NaBr (final concentration 100 mM). For 'with oxygen' solutions were X-irradiated without prior treatment; for 'without oxygen' solutions were deaerated by the 'freeze-pump-thaw' procedure.

#### $\bullet\text{OH}$ Radical with and Without Oxygen

Clearly, there is an indication of a pronounced oxygen effect on the yield of 8oxoG for reaction of  $\bullet\text{OH}$  with DNA (Figure 26). The accumulation of 8oxoG is drastically reduced in the absence of oxygen. This indicates that after formation of the 'fixed hole' oxygen aids in converting the G-OH adduct into 8oxoG (the second one-electron oxidation). Even in the absence of oxygen some formation of 8oxoG occurs. The reasons for that are unknown; one can hypothesize that either some residual amounts of oxygen are enough to create some 8oxoG or that there is an oxygen-independent channel of oxidation 8oxoG precursors.

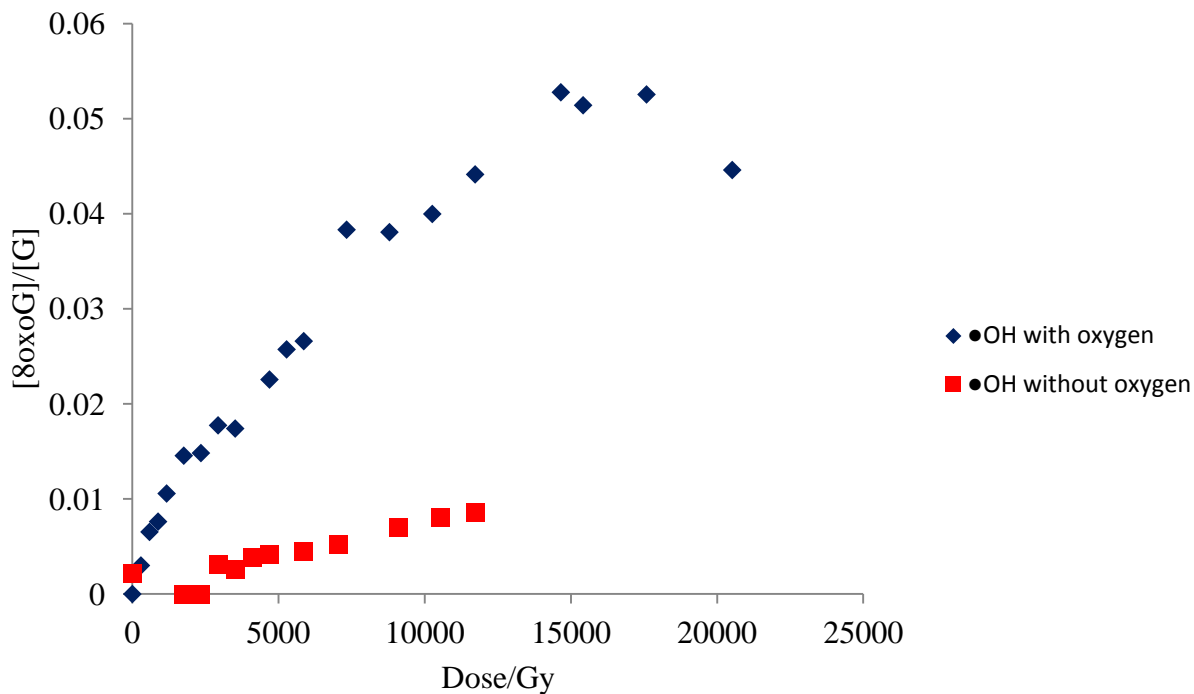


**Figure 26.** The effect of oxygen on the production of 8oxoG by hydroxyl radicals. Accumulation of 8oxoG from X-irradiated 10 mM solutions salmon testes DNA in the presence and absence of oxygen.

### Br<sub>2</sub>•<sup>-</sup> Radical with and Without Oxygen

These data present a very interesting and paradoxical situation (Figure 27). Unlike the experiment with •OH as a hole injector in which the yield of 8oxoG was greatly affected by oxygen, the experiments with Br<sub>2</sub>•<sup>-</sup> as a hole injector reproducibly showed even an increase in accumulation of 8oxoG without oxygen. It is difficult to interpret these unexpected results. Radiation chemical yields of •OH and Br<sub>2</sub>•<sup>-</sup> are believed to be very close because •OH is practically quantitatively converted into Br<sub>2</sub>•<sup>-</sup> Reactions 5-7 in Chapter 2 due to a very fast

occurrence of Reactions 5-7, with rate constants  $1 \times 10^{10} \text{M}^{-1} \text{s}^{-1}$ <sup>21</sup> and a large equilibrium constant for the formation of  $\text{Br}_2^{\bullet-}$  in Reaction 7 ( $3.9 \times 10^5$ ).<sup>84</sup>

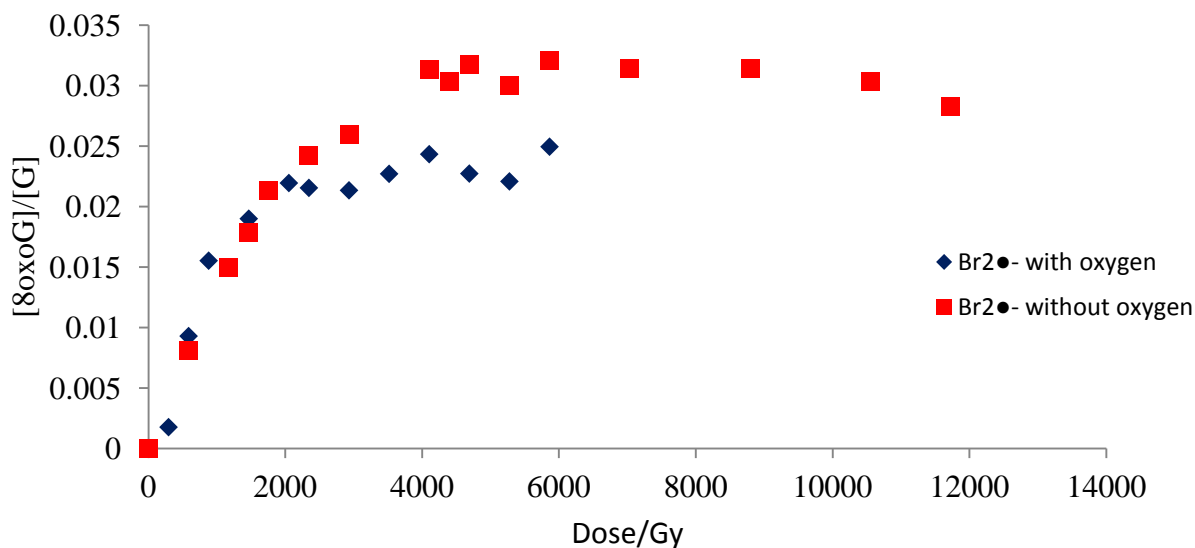


**Figure 27.** The effect of oxygen on the production of 8oxoG by hydroxyl radicals. Accumulation of 8oxoG from X-irradiated 10 mM solutions of salmon testes DNA with 100 mM NaBr in the presence and absence of oxygen.

Such a striking difference in oxygen effect of 8oxoG production for these two hole injectors likely lies in the difference of mechanisms of formation of 8oxoG: predominately via the  $\text{G}(\text{OH})^{\bullet}$  radicals in case of hydroxyl radicals and via the guanine radical cation in case of dibromide radical anions. Although it is currently believed that 8oxoG is formed from guanine radical cation via formation of the  $\text{G}(\text{OH})^{\bullet}$  radicals as an intermediate, it cannot be excluded that

there is a direct channel of conversion of guanine radical cation into 8oxoG, which may be oxygen-independent. Because guanine radical cations are mobile holes, it can be hypothesized that they can migrate towards the neighboring  $G(OH)^{\bullet}$  radicals formed via hydrolysis of guanine radical cations and oxidize them to form 8oxoG. In this model, oxygen as a second oxidant is not required. Apparently, this oxygen-independent formation of 8oxoG is possible only in the case of formation of mobile holes rather than 'fixed' holes. Thus, this model explains why production of 8oxoG can occur efficiently even under deoxygenated conditions when dibromide radical anions are used as hole injectors while it is essentially oxygen-dependent when hydroxyl radical are used as hole injectors.

### The Effect of G Content and Sequence of DNA on Production of 8oxoG

#### The Effect of G Content on Production of 8oxoG

Different types of DNA with various G-content were used to elucidate the effect of charge migration on the steady state production of 8oxoG. Two types of native DNA: salmon testes DNA (21% of G) and DNA from *Micrococcus Luteus* (36% of G), and four types of synthetic polymerized DNA: poly CG-GC and poly GG-CC (50% of G in both) have been used. For this set of experiments, 1 mM or 2.5mM (in nucleotides) solutions of different types of DNA in 10 mM phosphate buffer, pH 6.9, in the presence of 100mM NaBr were X-irradiated at indicated doses.

The plot of accumulation of 8oxoG with dose for 1 mM DNA is shown in Figure 21A. Figures 28-30 show individual plots for 8oxoG production for all other 3 types of DNA.

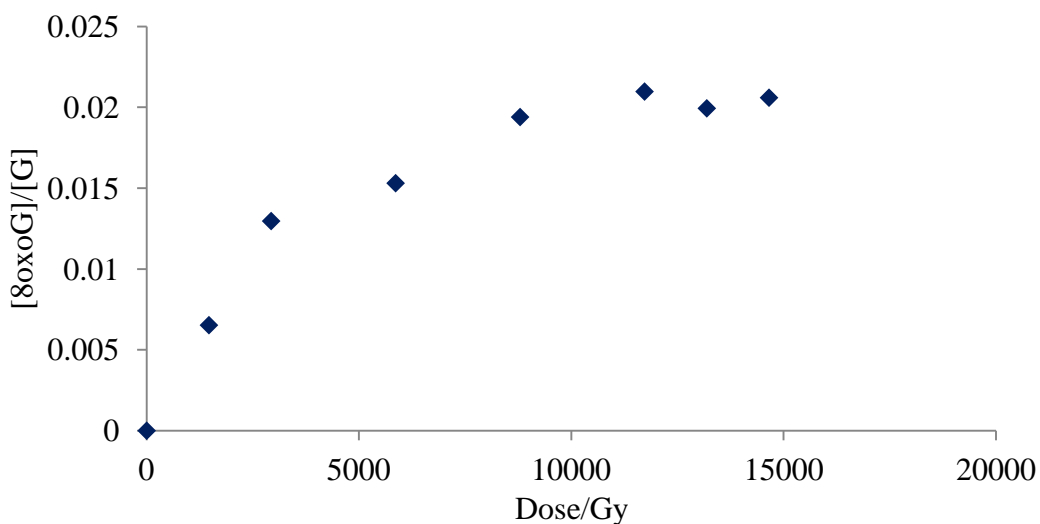


**Figure 28.** Accumulation of 8oxoG from X-irradiated 2 mM solution of micrococcal DNA in 10 mM phosphate buffer, pH 6.9, in the presence of 100m M NaBr. Post irradiation treatment and HPLC conditions were as previously described.

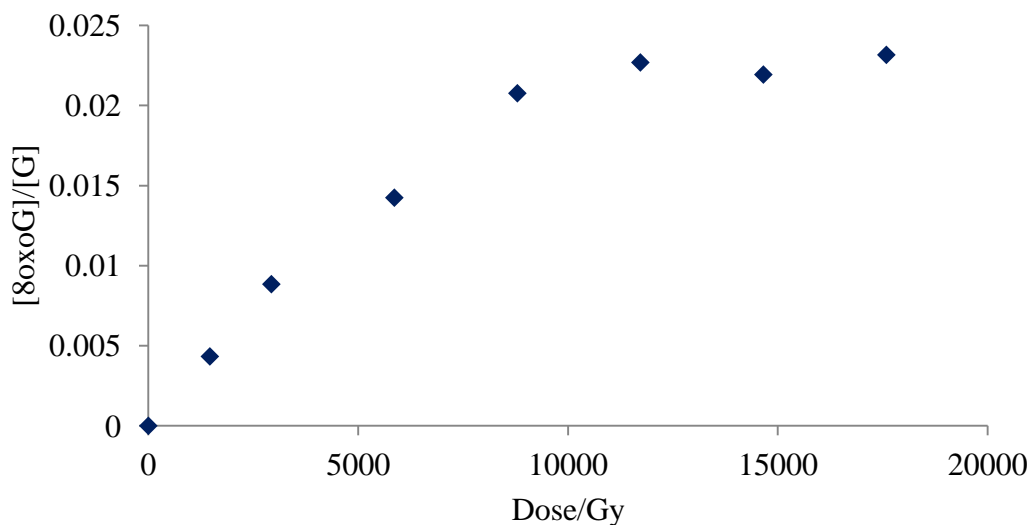


**Figure 29.** Accumulation of 8oxoG from X-irradiated 1 mM solution of poly (CG-GC). Other conditions are as in Figure 28.

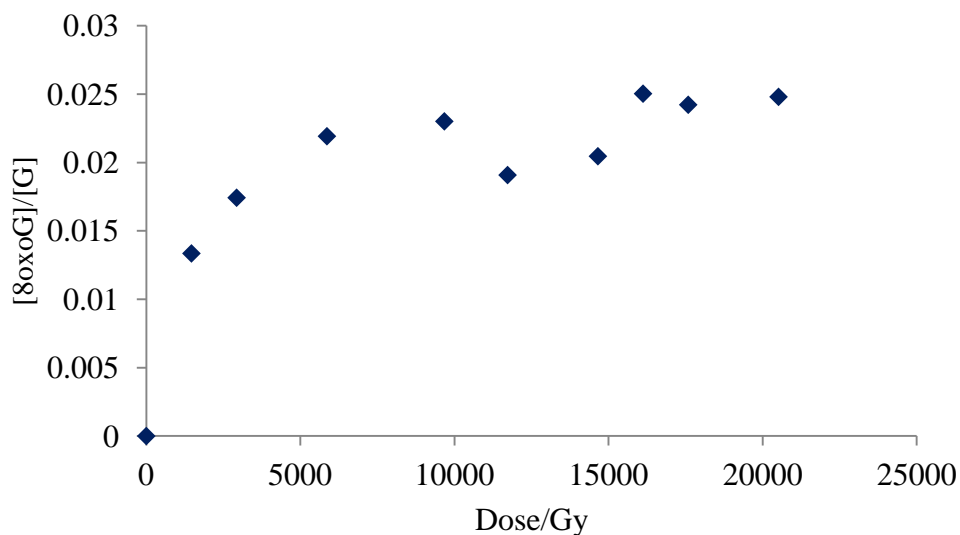


**Figure 30.** Accumulation of 8oxoG from X-irradiated 0.71 mM solution of poly(GG-CC). Other conditions are is in Figure 28.

As follows from Figures 28-30, both types of native DNA and both types of poly(GC) DNA show very similar levels of steady state yield of 8oxoG, in the range of 2.0-2.5% of total guanine.

The lack of dependence of steady state yield of 8oxoG on the G content is unexpected. According to Equation 13 in Chapter 2, the steady state ratio of  $[8oxoG]/[G] = X_{\infty}$  is proportional to the ratio of rate constant of reaction an diffusion of the hole:

$$k_r/k_d = 7.33 X_{\infty}^2 \quad (16)$$

The rate constant of diffusion,  $k_d$ , decreases with the increasing in the length of diffusion step, in its turn, is inversely proportional to the G content in DNA. So, it can be expected from the diffusion model that the steady state yield of 8oxoG should be lower in DNA with a higher



content of G, but no such correlation was observed for salmon testes DNA (21% G), micrococcal DNA (36% G), or both types of poly(GC) DNA (50% G). It can be concluded that the experimental data do not prove the mathematical model and that the likely reason for that is the existence of a more complex kinetic scheme for the formation and reactions of 8oxoG and that the suggested mathematical model is an oversimplification of a real mechanism.

Table 5 summarizes the data obtained in this section by presenting the average number of base pair (bp) per 8oxoG, i.e. an average distance in bp between two 8oxoG. This is helpful to assess the number of 8oxoG produced in each DNA type. The number of bp per 8oxoG for salmon testes DNA, 119 bp/8oxoG is a reasonably good agreement with earlier reported data by Cai and Sevilla,  $127 \pm 6$ <sup>30</sup> obtained under similar experimental conditions.

**Table 5:** Number of base pair per 8oxoG produced from different types of DNA

DNA type	Number of bp per 8oxoG
Salmon Testes DNA (1mM)	119
Micrococcal DNA (2.5mM)	46
Poly GG-CC	80
Poly GC-CG	100

## The Effect of DNA Sequence on Production of 8oxoG

The effect of DNA sequence on production of 8oxoG was elucidated by comparing yields of 8oxoG produced oxidation of poly(GC-CG) and poly(GG-CC) by dibromide radical anion. 1 mM or 0.71 mM (in nucleotides) of different types of DNA in 10 mM phosphate buffer, pH 6.9 and were X-irradiated at indicated doses in the presence of 100 mM NaBr (Figures 29 and 30).

As is evident from the comparison of Figures 29 and 30, both types of poly (CG) DNA show essentially the same steady state yield of 8oxoG, though the rate of initial accumulation of 8oxoG is faster for poly (GG-CC). Similar yields of 8oxoG for both types of poly (CG) DNA is not unexpected. As is evident from Figures 9 and 10 in Chapter 2, only intrastrand migration of holes along the G-strand is possible for poly (GG-CC), while for poly (GC-CG) both intrastrand migration and a zigzag interstrand migration between guanine can occur. Therefore, though the diffusion step in poly (GC-CG) is 2-fold longer than in poly (GG-CC), holes in poly (GC-CG) can also migrate in the interstrand fashion, which facilitates the hole migration.

Table 6 summarizes various DNA types, hole injectors, and  $k_d/k_r$  ratios calculated from experimental data using equation 13 in Chapter 2. It can be seen from this table that typically the  $k_d/k_r$  ratios are in the range of ~200-300 (with the exception of the carbonate radical anion), i.e. the diffusion rate constant is 200-300 times larger than the reaction rate constant. This implies that mobile holes created migrate much faster to the scavenging site 8oxoG than they do react to form new 8oxoG.

**Table 6.** The ratios of the rate constant of diffusion to the rate constant of reaction for holes in DNA calculated from experimental data

DNA	% G	Oxidant	[8oxoG]/[G] %	$k_d/k_r$
Salmon Testes	21	$\text{Br}_2^{\bullet-}$	2.5	218
Salmon Testes	21	$\text{SO}_4^{\bullet-}$	2.0	341
Salmon Testes	21	$\text{CO}_3^{\bullet-}$	1.0	1364
Micrococcus Letues	36	$\text{Br}_2^{\bullet-}$	2.0	341
Poly(GG-CC)	50	$\text{Br}_2^{\bullet-}$	2.5	218
Poly(GC) - Poly(CG)	50	$\text{Br}_2^{\bullet-}$	2.0	341

## CHAPTER 5

### CONCLUSIONS

1. In the present work, the kinetics of accumulation of 8oxoG as a result of oxidation of DNA by a number of oxidants (hole injectors) has been studied. Experimentally obtained values for the yields of 8oxoG were most typically in the range of 2.0 – 2.5% of the total concentration of guanine, in a good agreement with the previous values of  $1.9 \pm 0.1\%$ .<sup>30</sup>
2. It has been demonstrated that while such hole injectors as  $\text{Br}_2^{\bullet-}$ ,  $\text{SO}_4^{\bullet-}$ , and  $\text{CO}_3^{\bullet-}$  show similar patterns of kinetics of 8oxoG accumulation, in which the steady state levels for 8oxoG in the range of 1-2.5% of the total guanine are attained at relatively low doses,  $\bullet\text{OH}$  shows quite a different pattern, in which the steady state concentrations of 8oxoG are much higher (up to 20%) and that are reached at much higher doses. It has been hypothesized that the reason for different patterns in 8oxoG kinetics lies in different mechanisms of formation of 8oxoG precursors:  $\bullet\text{OH}$  predominantly forms stable G-OH adducts as 'fixed' holes not capable of charge migration that results in increased levels of 8oxoG accumulation.  $\text{Br}_2^{\bullet-}$ ,  $\text{SO}_4^{\bullet-}$ , and  $\text{CO}_3^{\bullet-}$  are believed to form mobile holes  $\text{G}^{\bullet+}$ , via direct inner sphere electron transfer in case of  $\text{Br}_2^{\bullet-}$  or via formation of unstable adducts with rapid elimination in case of  $\text{SO}_4^{\bullet-}$ , and  $\text{CO}_3^{\bullet-}$ . As a result, hole migration competes with its reaction of conversion into 8oxoG to produce lower amounts of 8oxoG.
3. There is no apparent correlation between the reduction potential of the oxidant and the steady state concentration of 8oxoG.

4. As expected from the diffusion model, DNA concentrations do not have any significant effect on the yield of 8oxoG. Once the hole is injected into a DNA array, its fate does not depend on DNA concentration.
5. Surprisingly, no correlation between the G content in DNA and the steady state yield of 8oxoG has been experimentally observed. Different types of DNA with different G content, such as salmon testes DNA (21% G), micrococcal DNA (36% G), and two types of poly(CG) DNA (50% G) showed very similar yields of 8oxoG, in the range of 2-2.5% of total G. These findings disagree with the prediction of the diffusion model, according to which the steady state levels of 8oxoG depend on the number of hole traps in DNA, i.e. on the G content. This disagreement implies that the actual kinetics of 8oxoG accumulation in DNA is more complicated than the model used in this study and predicts that a more advanced model is required to better accommodate experimental data. In particular, it might indicate that the use of only two reaction rate constants is an oversimplification of the real kinetics of 8oxoG in DNA.
6. The ratios of the hole reaction rate constant over the hole diffusion rate constant,  $k_d/k_r$  were estimated from the experimental data to be in the range of ~ 200-300, which implies that the hole diffusion occurs much faster than its conversion into 8oxoG, in general agreement with earlier findings.<sup>113</sup> However it is difficult to compare the values of the  $k_d/k_r$  ratio obtained in this work with those previously reported because apparently no correlation between the G content in DNA and the  $k_d/k_r$  ratios has been obtained in the present work.

## REFERENCES

1. Valko, M.; Morris, H.; Cronin, M. T. *Cur. Med. Chem* **2005**, *12*, 1161-1208.
2. Cadet, J.; Douki, T.; Pouget, J. P.; Ravanat, J. L.; Sauvaigo, S. *Curr. Probl. Dermatol.* **2001**, *29*, 62-73.
3. Cook, J. A.; Gius, D.; Wink, D. A.; Krishna, M. C.; Russo, A.; Mitchell, J. B. *Semin. Radiat. Oncol.* **2004**, *14*, 259-266.
4. Miura, Y. *J. Radiat. Oncol.* **2004**, *14*, 259-266.
5. Schmidt-Ullrich, R. K.; Dent, P.; Grant, S.; R.B, M.; Valerie, K. *Radiat. Res.* **2000**, *153*, 245-257.
6. Demarini, D. M. *Mutat, Res* **2004**, *567*, 447-474.
7. Pryor, W. *Environmental Health Perspective* **1997**, *105*, 875-882.
8. Burrows, C. J.; Muller, J. G. *Chem. Rev.* **1998**, *98*, 1109-1151.
9. Cullis, P. M.; Malone, M. E.; Merson-Davies, L. A. *J. Am. Chem. Soc.* **1996**, *118*, 2775-81.
10. Barry, H. *Bio Chem.J.* **2007**, *401*.
11. Evans, M. D.; Dizdaroglu, M.; Cooke, M. S. *Mutat. Res* **2004**, *574*, 1-61.
12. Wiseman, H.; Halliwell, B. *Biochem. J.* **1996**, *313*, 17-29.
13. Lezza, A.; Mecocci, P.; Cormio, A.; Flint Beal, M.; Cherubini, A.; Cantatore, P.; Senin, U.; Gadaleta, M. N. *J. AntiAging Med* **1999**, *2*, 209-215.
14. Lovell, M. A.; Gabbita, S. P.; Markesbery, W. R. *J. Neurochem.* **1999**, *72*, 771-776.
15. Zhang, J.; Perry, G.; Smith, M.; Robertson, D.; Olson, S. J.; Graham, D. G.; Montine, T. J. *Am. J. Pathol.* **1999**, *154*, 1423-1429.

16. Alam, Z.; Jenner, A.; Daniel, S. E.; Lees, A. J.; Cairns, N.; Marsden, C. D.; Jenner, P.; Halliwell, B. *J. Neurochem* **1997**, *69*.
17. Loft, S.; Larsen, P. N.; Rasmussen, A.; Fischer-Nielsen, A.; Bondesen, S.; Kirkegaard, P.; Rasmussen, L. S.; Ejlersen, E.; Tornøe, K.; Bergholdt, R. *Transplantation* **1995**, *59*, 16-20.
18. Tokokuni, S. *International Union of Biochem. Mol. Biol, Life* **2008**, *60*, 441-447.
19. Yang, Y.; Tian, Y.; Yan, C.; Jin, X.; Shen, X. *Environ. Toxicol.* **2008**.
20. Das T.N.; Dhanasekaran T.; Alfassi Z.B.; Neta P. Reduction potential of the tert-butylperoxyl radical in aqueous solutions. In: Proceedings of the 4th International Conference on Chemical Kinetics; **1997**; Gaithersburg, Md, USA. National Institute of Standards and Technology.
21. Von Sonntag, C. *Free-radical-induced DNA Damage and its Repair* New York: Springer-Verlag, Berlin Heidelberg, 2010.
22. Steenken, S.; Jovanovic, S. V.; Bietti, M. *J. Am. Chem. Soc.* **2000**, *122*, 2373-2374.
23. Milligan, J. R.; Aguilera, J. A.; Nguyen, J. V.; Ward, J. F. *Int. J. Radiat. Biol.* **2001**, *77*, 281-293.
24. Steenken, S.; Jovanovic, S. V. *J. Am. Chem. Soc.* **1997**, *119*, 617-618.
25. Regnisson, J.; Steenken, S. *Phys. Chem. Chem. Phys* **2002**, *4*, 527-532.
26. Milligan, J. R.; Aguilera, J. A.; Hoang, O.; Tran, N. Q.; Ward, J. F. *J. Am. Chem. Soc.* **2004**, *126*, 1682-1687.
27. Steenken, S. *Free Rad Res Comm* **1992**, *16*, 349-379.
28. Close, D. M. *J. Phys. Chem. A* (2013), *117*(2), 473-480
29. Saito, I.; Nakamura, T.; Nakatani, K.; Yoshioka, Y.; Yamaguchi, K.; Sugiyama, H. *J. Am. Chem. Soc.* **1998**, *120*, 12686-12687.

30. Cai, Z.; Sevilla, M. D. *Radiat. Res.* **2003**, *159*, 411-419.
31. Cadet, J.; Douki, T.; Gasparutto, D.; Ravanat, J. L. *Mut. Res.* **2003**, *531*, 5-23.
32. Douki, T.; Martini, R.; Ravanat, J. L.; Turesky, R. J.; Cadet, J. *Carcinogenesis* **1997**, *18*, 2385-2391.
33. Simon, W. C.; Dedon, C. P. *J. Nucleic Acids.* **2010**, *2010*, 13.
34. Doddridge, Z. A.; Cullis, P. M.; Jones, G. D. D.; Malone, M. E. *J. Am. Chem. Soc.* **1998**, *120*, 10998-10999.
35. Close, David M.; Nelson, William H.; Bernhard, William A. *J. Phys. Chem. A* (2013), *117*(47), 12608-12615.
36. Saito, I.; Takayama, M.; Sugiyama, H.; Nakatani, K. *J. Am. Chem. Soc.* **1995**, *117*, 6406-6407.
37. Lewis, F. D.; Liu, X.; Liu, J.; Hayes, R. *J. Am. Chem. Soc.* **2000**, *122*, 12037-12038.
38. Giese, B. A.; Amdrut, J.; Kohler, A. K.; Spormann, M.; Wessely, S. *Nature* 2001, *412*, 318-320.
39. Bonne, E.; Schuster, G. B. *Nucleic Acids Res.* **2002**, *30*, 830-837.
40. Conwell, E. M.; Basko, D. M. *J. Am. Chem. Soc.* **2001**, *123*, 11441-11445.
41. Asami, S. H., T. Yamaguchi, R. Tomioka Y, Itoh H, Kasai, H. *Cancer Res.* **1996**, *56*, 2546-2549.
42. Kiyosawa, H. S.; M. Okudaira H.; Murata K.; Miyamoto T.; Chung MH.; Kasai H.; *Free Radic. Res. Commun.* **1990**, *11*, 23-27.
43. Jackson, J. S., IU. Hyslop PA, Vosbeck, K. Sauerheber, R. Weitzman, SA. Cochrane, CG. *J. Clin. Invest.* **1987**, *80*, 1090-1095.
44. Chen, Q. M.; J. Ames, B.; Mossman, B.; *Carcinogenesis* **1996**, *17*, 2525-2527.
45. Valavanidis, A.; Vlachogianni, T.; *J. Environ. Sci. Health Part C* **2009**, *27*, 120-139.



46. Pope, C. I. B. R.; Thun, M.J.; Calle, E.E.; Krewski, D.; Thurston, G.D.; *J. Amer. Med. Associat.* **2002**, *287*, 1132-1141.
47. Kasprzak, K. *Free Rad. Biol.Med.* **2002**, *32*, 958-967.
48. Marczymski, B.; R., P.; Mensing, T.; Angerer, J.; Seidel, A.; El Mourabit, A.; Wilhelm, M.; Bruning, T. *Int. Arch. Occup. Environ. Health.* **2005**, *78*, 97-108.
49. Marczymski, B.; Rihs, H.; Rossbeach, B.; Holzer, J.; Angerer, J.; Scherenberg, M.; Hoffmann, G.; Bruning, T.; Wilhelm, M. *Carcinogenesis* **2002**, *23*, 273-281.
50. Toraason, M.; Hayden, C.; Marow, D.; Rinehart, R.; Mathgias, P.; Werren, D.; DeBord, D.; Reid, T. *Int. Arch. Occup. Environ. Health.* **2001**, *74*, 396-404.
51. Zhang, J.; Ichiba, M.; Hanaoka, T.; Pan, G.; Yamano, Y.; Hara, K.; Takahashi, K.; Tomokumi, K. *Int. Arch. Occup. Environ. Health.* **2003**, *79*, 499-504.
52. Steve, D. B.; Derek, N. P. G.; Verdine, G. L. Article Structural Basis for Recognition and Repair of the Endogenous Mutagen 8oxoG in DNA, *Nature*, **2000**, *403*, 859-866.
53. Grollman, A. P.; Takeshita, M. Miscoding and mutagenic properties of 8-oxoguanine and abasic sites: ubiquitous lesions in damaged DNA *SO Radiat. Damage DNA* **1995**, *61*, 293-304
54. Kasai, H.; Iwamoto-Tanaka, N.; Miyamoto, T.; Kawanami, K.; Kawanami, S.; Kido, R.; Ikeda, M. *Japan. J. Cancer Res.* **2001**, *92*, 9-15.
55. Giese, B. *Acc. Chem. Res.* **2000**, *33*, 631-636.
56. Shafirovich, V.; Cadet, J.; Gasparutto, D.; Dourandin, A.; Huang, W.; Geacintov, N. E. *J. Phys. Chem. B* **2001**, *105*, 586-592.
57. Wardman, P. *J. Phys. Chem. Ref*, **1989** *18*, 1637-1755.
58. Duarte, V.; Gasparutto, D.; Yamaguchi, L. F.; Ravanat, J. L.; Martinez, G. R.; Medeiros, M.

- H. G.; Mascio, P. D.; Cadet, J. *I. Am. Chem. Soc* **2000**, *122*, 12622-12628.
59. Burney, S.; Niles, J. C.; Dedon, P. C.; Tannenbaum, S. R. *Chem. Res. Toxicol.* **1999**, *12*, 513-520.
60. Tretyakova, N. Y.; Nile, J. C.; Burney, S.; Wishnok, J. S.; Tannenbaum, S. R. *Chem. Res. Toxicol.* **1999**, *12*, 459-466.
61. Luo, W.; Muller, J. M.; Rachlin, E. M.; Burrow, C. J. *Chem, Res. Toxicol.* **2001**, *14*, 927-938.
62. Duarte, V.; Muller, J. G.; Burrows, C. J. *Nucleic Acid Res.* **1999**, *27*, 496-502.
63. Luo, W.; Muller, J. G.; C.J, B. *Org. Lette.* **2000**, *2*, 613-616.
64. Niles, C. J.; Burney, S.; Singh, S. P.; Winshnok, J. S.; Teannenbaum, S. R. *Proc. Natl. Acad. Sci. USA* **1999**, *96*, 11729-11734.
65. Niles, C. J.; Winshnok, J. S.; Teannenbaum, S. R. *Chem. Res. Toxicol.* **2000**, *13*, 390-396.
66. Sheu, C.; Foote, C. S. *J. Am. Chem. Soc.* **1995**, *117*, 474-477.
67. Sheu, C.; Foote, C. S. *J. Am. Chem. Soc.* **1995**, *117*, 6439-6442.
68. Von Sonntag, C. *The Chemical Basis of Radiation Biology*; Taylor and Francis: New York, 1987.
69. Dizdaroglu, M. *Mutat, Res* **2005**, *591*, 45-59.
70. Demple, B. Sung, J. S. *DNA Repair (Amst)* **2005**, *4*, 1442-1449.
71. Fridberg, E. C. Walker, G. C.; Siede, W. *DNA Repair Mutagenesis.*; ASM Press: Washington DC, 1995.
72. Slupphaug, G. Kavli, B. H.E., K. *Mutat. Res.* **2003**, *531*, 231-251.
73. Shigenaga, R. Gimeno, C.; Ames, B. *PNAS* **1989**, *86*, 9697-9701.
74. Cooke, M. J, L. Evans, M. *Free Rad. Biol. Med.* **2002**, *33*, 1601-1614.

75. Serrano, J. Palmeria, C. Wallace, K. Kuehl, D. *Rapid Communication Mass Spectrometry* **1996**, *10*, 1789-1791.
76. Dizdaroglu, M. Jaruga, P.; Birincioglu, M.; Rodringuez, H. *Free Rad. Biol. Med.* **2002**, *32*, 1102-1115.
77. Kasai, H. *J. Rad. Res.* **2003**, *44*, 185-189.
78. Wagenknecht, H. A. *Angew. Chem. Int. Ed. Engl.* **2003**, 2454-2460.
79. Eley, D. D. Spivey, I. D. *Trans. Faraday. Soc.* **1962**, *58*, 411-415.
80. Gasper, S. M. Schuster, G. B. *J. Am. Chem. Soc.* **1997**, *119*, 12762-12771.
81. Ly, D. Sanii, L.; Schuster, G. B. *J. Am. Chem. Soc.* **1999**, *121*, 9400-9410.
82. Meggers, E.; Kusch, D.; Spichty, M.; Wille, U.; Giese, B. *Angew. Chem., Int. Ed.* **1998**, *37*, 460-462.
83. Henderson, P. T. Jones, D.; Hampikian, G.; Kan, Y. *Proc. Natl. Acad. Sci. U. S. A.* **1999**, *96*, 8353-8358.
84. Lui, Y.; Pimentel, A. S.; Antoku, Y.; JR, B. *J. Phys. Chem. A* **2002**, *106*, 11075-11082.
85. Ly, D. Kan, Y.; Armitage, B.; Schuster, G. B. *J. Am. Chem. Soc.* **1996**, *118*, 8747-8748.
86. Kino, K. Saito, I. *J. Am. Chem. Soc.* **1998**, *120*, 7373-4.
87. Stemp, E. D. A. Arkin, M. R.; Barton, J. K. *J. Am. Chem. Soc.* **1997**, *119*, 2921-2925.
88. Arkin, M. R.; Stemp, E. D. A.; Pulver, S. C.; Barton *Chem. Biol.* **1997**, *4*, 389-400.
89. Muller, J. G.; Hickerson, R. P.; Perez, R. J.; Burrows, C. J. *J. Am. Chem. Soc.* **1997**, *119*, 1501-1503.
90. Kelley, S. O.; Barton, J. K. *Science* **1999**, *283*, 375-381.
91. Brun, A. M.; Harriman, A. *J. Am. Chem. Soc.* **1992**, *114*, 3656-3660.

92. Kelley, S. O.; Holmlin, R. E.; Stemp, E. D. A.; Barton, J. K. *J. Am. Chem. Soc.* **1997**, *119*, 9861-9870.
93. Kelley, S.; Barton, J. *Chem. Biol.* **1998**, *5*, 413-25.
94. Fukui, K.; Tanaka, K. *Angew. Chem. Int. Ed.* **1998**, *37*, 158-161.
95. Lewis, F. D.; Liu, X.; Wu, Y.; Miller, S. *J. Am. Chem. Soc.* **1999**, *121*, 9905-9906.
96. Nakatani, K.; Dohno, C.; Saito, I. *J. Am. Chem. Soc.* **1999**, *121*, 10854-10855.
97. Giese, B.; Wessely, S.; Spormann, M.; Lindemann *Angew. Chem., Int. Ed.* **1999**, *38*, 996-998.
98. Bhaskar, G. M.; Ramaserna, T. *School of Chemistry University of Hyderabad, Department of Biochemistry, India Institute of Science, Bangalore India* **2001**, *80*.
99. Lewis, F. Liu, J.; Weigel, W. Rettig, W. IV, K. DN, B. *Proc Natl Acad Sci* **2002**, *99*, 12536-12541.
100. Turro, N. J.; Barton, J. K., *J. Biol. Inorg. Chem.* **1998**, *3*, 201-209.
101. Priyadarshy, S.; Risser, S. M.; Beratan, D. N. *J. Phys. Chem.* **1996**, *100*, 17678-82.
102. Harriman, A. *Angew. Chem. Int. Ed.* **1999**, *38*, 945-948.
103. Debije, M. G.; Milano, M. T.; Bernhard, W. A. *Angew. Chem., Int. Ed.* **1999**, *38*, 2752-2756.
104. Beratan, D. N.; Priyadarshy, S.; Risser, S. M. *Chem. Biol.* **1997**, *4*, 3-8.
105. Nunez, M. E.; Hall, D. B.; Barton, J. K. *Chem. Biol.* **1999**, *6*, 85-97.
106. Henderson, P. T.; Jones, D.; Hampikian, G.; Kan, Y.; Schuster, G. B. *Proc. Natl. Acad. Sci. USA* **1999**, *96*, 8353-8358.
107. Warman, J. M.; de Haas, M. P.; Rupprecht, A. *Chem. Phys. Lett.* **1996**, *249*, 319-22.
108. Hall, D. B.; Holmlin, R. E.; Barton, J. K. *Nature* **1996**, *382*, 731-735.

109. Jortner, J.; Bixon, M.; Langenbacher, T.; Michel-Beyerle, M. E. *Proc. Natl. Acad. Sci* **1998**, *95*, 12759-12765.
110. Liu, C. S.; Hernandez, R.; Schuster, G. B. *J. Am. Chem. Soc* **2004**, *126*, 2877-2884.
111. Meggers, E.; Michel-Beyerle, M. E.; Giese, B. *J. Am. Chem. Soc.* **1998**, *120*, 12950-12955.
112. Razskazovskii, Y.; Swarts, S. G.; Falcone, J. M.; Taylor, C.; Sevilla, M. D. *J. Phys. Chem* **1997**, *101*, 1460-1467.
113. Roginskaya, M.; Bernhard, W. A.; Razskazovskiy, Y. *J. Phys. Chem. B* **2004**, *108*, 2432-2437
114. Joffe, A.; Geacintov, N. E.; Shafirovich, V. *Chem. Res. Toxicol.* **2003**, *16*, 1528-1538.
115. Crean, C.; Lee, Y. A.; Yun, B. H.; Geacintov, N. E.; Shafirovich, V. *Chem, Bio, Chem* **2008**, *9*, 1985-1991.
116. Zehavi, D.; Rabani, J. *J Phys Chem* **1972**, *76*, 312-319.
117. Milligan, J. R.; Aguilera, J.; Paglinawan, R. A.; J.F, W. *Int J Radiat Biol* **2002**, *78*, 359-374.
118. Liebe, F.; Bendick, A. **1950**, *72*, 2587-2594.
119. Martin, R. F.; Anderson, R. F. *Int. J. Radiat. Oncol., Biol., Phys.* **1998**, *42*, 827-831.
120. Basolo, F.; Murmann, R. K. *Lnorg. Synt* **1953**, *4*, 171-171.
121. Fricke, H.; Hart, E. J. *Chemistry Dosimetry*; Academic Press: New York, 1966.

## APPENDICES

### APPENDIX A

#### Determination of Extinction Coefficient of 8oxoG at 305nm

Using the Beer-Lambert law:

$$(A_{305}/A_{285}) = ([8oxoG]_{305} \times \epsilon_{305} \times b) / ([8oxoG]_{285} \times \epsilon_{285} \times b)$$

The extinction coefficient of 8oxoG at 305nm was determined as is described in Chapter 3. UV-Vis spectra of a series of dilutions of saturated solution of 8oxoG were obtained and absorbencies at 305 nm were plotted as a function of absorbencies at 285 nm (Figure 15). The gradient that gave 0.4453 was used in the calculation below to obtain the extinction coefficient of 8oxoG at 305 nm.

$$\epsilon_{305} = \epsilon_{285} \times \text{slope} (A_{305}/A_{285}) = 7762.47 \times 0.4453 = 3458.59 \text{ M}^{-1} \text{ cm}^{-1}$$

## APPENDIX B

### Fricke Dosimetry

The dose rate was calculated using the Beer-Lambert law as

$$A_{305} = [Fe^{3+}] \times \epsilon_{304} \times b$$

$$\frac{\partial A}{\partial t} = \frac{\partial [Fe^{3+}]}{\partial t} \times \epsilon_{304} \times b$$

$\frac{\partial A}{\partial t}$  = the rate of change of absorbance with time (slope)

$\frac{\partial [Fe^{3+}]}{\partial t}$  = the rate of accumulation of  $Fe^{3+}$  with time

$\frac{\partial [Fe^{3+}]}{\partial t}$  is related to the  $\rho G \partial D / \partial t$

Where  $\rho$  = the density of mixture, which is typically 1 kg/L, G is the radiation chemical yield of  $Fe^{3+}$  that is  $1.67 \times 10^{-6}$  mol/J, D is the dose rate Gy/s

The equation comes up to be

$$\frac{\partial D}{\partial t} = \frac{\frac{\partial A}{\partial t}}{\epsilon_{304} \rho G}$$

The constants comes up to =  $(1 \text{ kg/L} \times 1.5 \times 10^{-6} \times \text{mol/J} \times 2201 \text{ M}^{-1} \text{cm}^{-1} \times 1 \text{cm})^{-1} = 301.66 \text{ J/kg (Gy)}$

$$\frac{\partial D}{\partial t} = \frac{\partial A}{\partial t} \times 301.66$$

$$\frac{\partial D}{\partial t} = 9.77 \text{ Gy/s}$$

## APPENDIX C

### The Linear Regression for the Initial Accumulation of Different DNA Concentrations

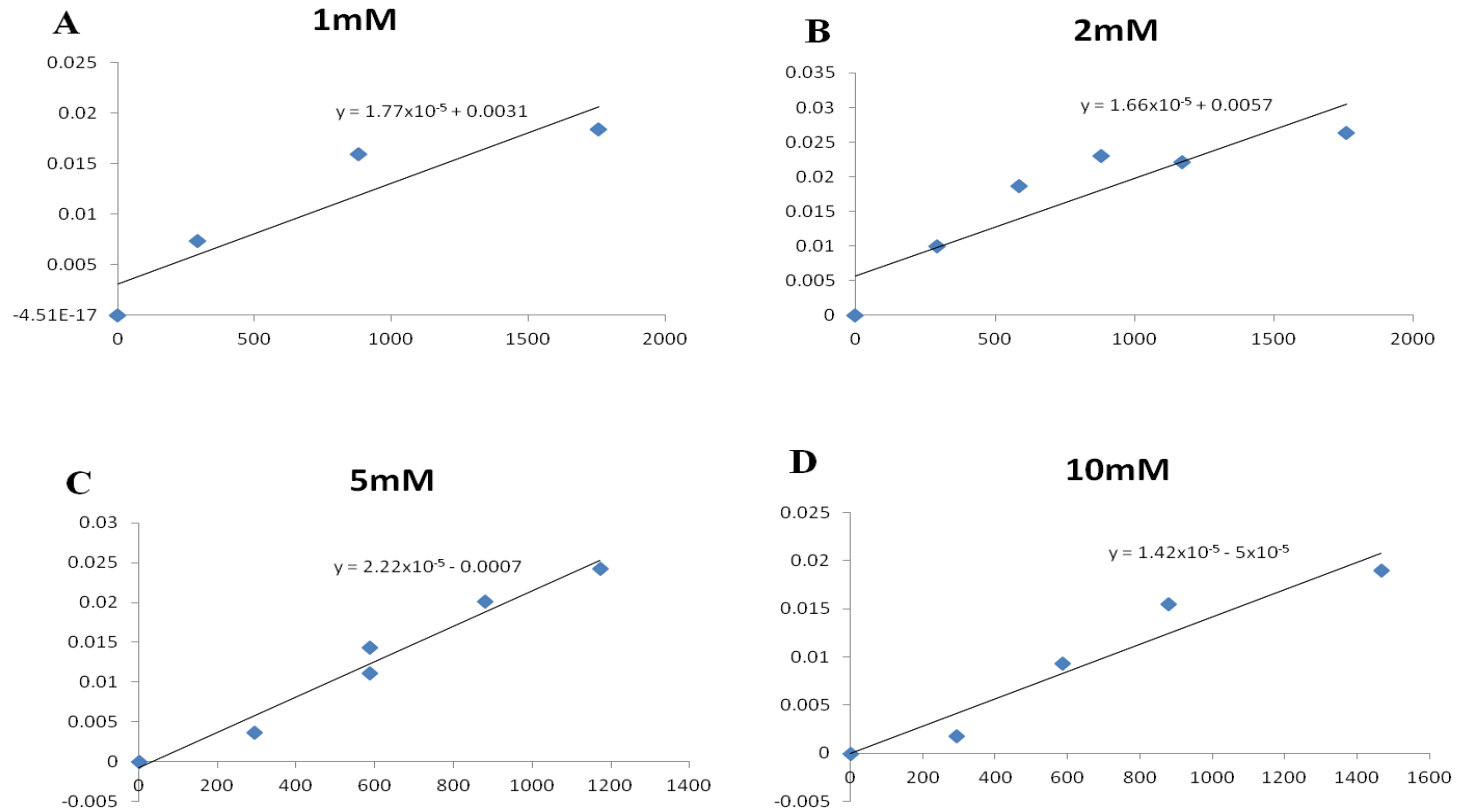


**Figure 31:** The linear regression for the initial accumulation of different DNA concentrations; **A.** 1mM, **B.** 2mM, **C.** 5mM and **D.** 10mM



## VITA

### DERRICK AMPADU BOATENG

- Personal Data:                   Date of Birth: January 19, 1983
- Place of Birth: Accra, Ghana
- Marital Status: Married
- 
- Education:                        BS Chemistry, Nkrumah University of Science and Technology, 2006
- Kumasi, Ashanti Region Ghana
- Diploma in Business Management and Administration, Institute of
- Commercial Management (ICM), 2009 UK
- Diploma in Financial Management, Institute of Commercial
- Management (ICM), 2009 UK
- M.S. Chemistry, East Tennessee State University, 2014
- Johnson City, Tennessee USA
- 
- Professional Experience: Undergraduate research, Ghana Standard Board, Greater Accra Region
- Accra, Ghana, 2005-2006
- Teacher, Nsawam Senior High School, Nsawam, Eastern Region,
- Ghana, 2006-2008
- Quality Control Chemist, Letap Pharmaceuticals Limited
- Greater Accra Region, Accra, Ghana, 2009-2012

Graduate Assistant, East Tennessee State University, Jonson City  
Tennessee, Chemistry Department, 2012-201